

Contents lists available at ScienceDirect

# Geoderma

journal homepage: www.elsevier.com/locate/geoderma





# Root distributions, precipitation, and soil structure converge to govern soil organic carbon depth distributions

Ligia F.T. Souza <sup>a,b,\*</sup>, Daniel R. Hirmas <sup>c</sup>, Pamela L. Sullivan <sup>d</sup>, Daniel C. Reuman <sup>a,b</sup>, Matthew F. Kirk <sup>e</sup>, Li Li <sup>f</sup>, Hoori Ajami <sup>g</sup>, Hang Wen <sup>h</sup>, Marcos V.M. Sarto <sup>i</sup>, Terry D. Loecke <sup>b,j</sup>, Aoesta K. Rudick <sup>b</sup>, Charles W. Rice <sup>e</sup>, Sharon A. Billings <sup>a,b</sup>

- <sup>a</sup> Department of Ecology and Evolutionary Biology, University of Kansas, 66045 Lawrence, KS, USA
- <sup>b</sup> Kansas Biological Survey and Center for Ecological Research, University of Kansas, 66047 Lawrence, KS, USA
- <sup>c</sup> Department of Plant and Soil Science, Texas Tech University, 79409 Lubbock, TX, USA
- <sup>d</sup> College of Earth, Ocean and Atmospheric Science, Oregon State University, 97331 Corvallis, OR, USA
- e Department of Geology, Kansas State University, 66506 Manhattan, KS, USA
- f Department of Civil and Environmental Engineering, Penn State University, 16801 University Park, PA, USA
- g Department of Environmental Sciences, University of California Riverside, 92521 Riverside, CA, USA
- <sup>h</sup> School of Earth System Science, Tianjin University, 300072 Tianjin, China
- <sup>i</sup> Department of Agronomy, Kansas State University, 66506 Manhattan, KS, USA
- <sup>j</sup> Environmental Studies Program, University of Kansas, 66045 Lawrence, KS, USA

#### ARTICLE INFO

Handling Editor: Alberto Agnelli

Keywords:
Soil aggregates
Subsoil
Organic carbon stabilization
Land use change
Anthropocene

#### ABSTRACT

The depth distribution of soil organic carbon (SOC) is governed by the interaction of many ecosystem features, including differential C inputs in shallow and deep soils and the redistribution of C via water flow through the profile. In C-rich Mollisols in particular, we need to better understand the degree to which the conversion of native prairie to cultivated lands is changing C loss and retention. We probed multiple mechanisms driving these processes using two approaches: one leverages a regional-scale dataset derived from the Natural Resources Conservation Service (USDA-NRCS) National Cooperative Soil Survey (NCSS) Characterization Database; and a second focusses on a local-scale, more detailed dataset representative of the climatic and land-use gradients invoked in the larger database. The first approach focused on parameterizing SOC depth distributions of Mollisols across a climatic gradient in the US Midwest to investigate how land use and effective precipitation affects vertical gradients of SOC. The second approach furthered the investigation of SOC depth distribution drivers by quantifying biological, physical, and chemical properties of multiple soil profiles across Kansas, US. SOC declined more gradually with depth as water availability increased in native prairie soils, prompting the hypothesis that increased water flow through the profile carries C to deep layers, particularly where high root abundances promote soil porosity. Analyses of multiple soil profiles indicate that surficial changes driven by land conversion propagate their influence to deep soil horizons in ways significant for the coupling of C cycling across depths. Our findings support the hypothesis, and specifically suggest linkages between decreased root abundances and increased flows of soluble C downward under agriculture, and associated changes in soil structure that affect the propensity of SOC to form aggregates. The interplay between rooting depth abundances and water availability in different land uses thus appears to influence the arrangement of soils particles and voids in ways important for vertical water flow and C transport. Our work illuminates the convergence of multiple important mechanisms driving changes in the shape of SOC depth distributions across timescales shorter than typically assumed, with consequences for projecting soil C cycling and storage in the Anthropocene.

<sup>\*</sup> Corresponding author at: Department of Earth Sciences, Memorial University of Newfoundland, A1C5S7 St. John's, NL, Canada. *E-mail address*: ligiaftsouza@mun.ca (L.F.T. Souza).

#### 1. Introduction

The majority of organic carbon (C) in terrestrial ecosystems resides in soils (Jobbágy and Jackson, 2000; Lal, 2003; Jackson et al., 2017). Chemical, physical, and biological drivers are combined to influence soil organic carbon (SOC) stocks (Jackson et al., 2017). Decades of research emphasize the role of climate (Davidson et al., 2000; Lal, 2004; Davidson and Janssens, 2006; Bradford et al., 2016; Crowther et al., 2016) and land-use change (e.g., conversion of native systems to agriculture; Conant et al., 2017; Deng et al., 2016; Guo and Gifford, 2002; Tang et al., 2019) as drivers of SOC transformations. A key motivating factor in many of these and related studies is the potential feedback of SOC mineralization to atmospheric CO2. However, the stabilization or destabilization of SOC also governs another, less-appreciated but important driver of land-atmosphere feedbacks. Specifically, changes in SOC form and content can modify soil structure (Tisdall and Oades, 1982; Six et al., 2000; Loveland and Webb, 2003; Schwendenmann and Pendall, 2006; Meurer et al., 2020; Sullivan et al., 2022), which can further influence water storage, flow and land surface fluxes (Rawls et al., 2003; Minasny and McBratney, 2018) thus impacting ecosystem productivity (Banwart et al., 2019; Fatichi et al., 2020).

The idea that SOC and its biotic generation and transformation can influence soil structure and thus subsurface hydrologic flow paths is well-founded, and such transformations may occur across timescales far shorter than historically thought (Sullivan et al., 2022). For example, root activities and other C inputs to a soil profile can promote aggregate structure (Gould et al., 2016; Le Bissonnais et al., 2018). Such processes govern the structure of soil pore networks, which in turn modify water flow and nutrient transport, potentially affecting ecosystem productivity (Yudina and Kuzyakov, 2019). It is well-documented that soils with high organic matter (OM) content reduce bulk density (Haynes and Naidu, 1998; Ruehlmann and Körschens, 2009; Meurer et al., 2020), and influence the pore network architecture via the formation of aggregates as organic compounds act as binding agents linking soil mineral particles to each other (Six et al., 2004; Bronick and Lal, 2005). In spite of the link between SOC content and soil structure, relatively few studies have investigated the importance of interactions between biotically-mediated SOC stores and soil structure, especially deep in the subsurface (Banwart et al., 2011; Banwart et al., 2019; Brantley et al., 2017). To do so, and to make associated inferences about ecosystem functioning, requires understanding of these interacting phenomena in both surface and deep horizons (Rumpel and Kögel-Knabner, 2011; Sulman et al., 2020).

The depth distribution of SOC is governed by multiple, interacting features. Roots serve as a key C input, connecting the soil to the atmosphere and exerting control on the distribution of resources for biota -via water, nutrients, and gasses transport— throughout soils (Hinsinger et al., 2009). While rooting depth of the vegetation is perhaps the most intuitive driver of SOC inputs, its depth distribution is also governed by water availability, through multiple pathways. Water availability affects soil moisture that in turn dictates ecosystem productivity, and thus C inputs. Water availability, dictated in part by the balance between precipitation (P) and evapotranspiration (ET) demands, affects soil moisture and thus C inputs to the soil. Precipitation inputs often translate into hydrological flows through soil profiles that also can promote the movement of mobile SOC pools such as dissolved and particulate organic matter (DOM, POM) through soils (Kaiser and Kalbitz, 2012; Marín-Spiotta et al., 2014; Bowering et al., 2023). Rooting systems and water availability interactions control the spatial distribution of soil moisture whether by promoting hydraulic lift (Caldwell et al., 1998; Schenk and Jackson, 2002; Hinsinger et al., 2009) or forming preferential flow paths through which water can infiltrate (Hinsinger et al., 2009; Lu et al., 2020). These processes affect wetting and drying cycles that can move soil (Lu et al., 2020; Sullivan et al., 2022), influencing soil porosity and thus SOC transport throughout soil profiles (Jobbágy and Jackson, 2000). Soil texture modulates the capacity of a soil to move water, with relatively high clay concentrations offering greater resistance to water flow in many soils (Tisdall and Oades, 1982; Saxton et al., 1986; Saxton and Rawls, 2006). The presence or absence of roots and their capacity to redistribute water thus interacts with multiple soil attributes to direct temporally-variable soil structure and its capacity to protect C (Sullivan et al., 2022).

Because roots serve as an input of soil C and influence soil structure in ways that affect soil water dynamics, the interplay between root abundance, available moisture, and soil structure likely plays an important role in SOC depth distributions. For example, as C allocation belowground varies and deep root densities decrease upon the conversion of perennial systems to annual crops (Canadell et al., 1996; Jackson et al., 2000; Fan et al., 2016; Billings et al., 2018, Hauser et al., 2022), the associated formation of granular soil structure can be inhibited (Mohammed et al., 2020), likely affecting water flow (Sullivan et al., 2022) and the transport of DOC from surface to the subsurface (Kalbitz and Kaiser, 2008; Kaiser and Kalbitz, 2012; Podrebarac et al., 2021). The degree to which changes in rooting systems affect soil structure will depend on the rate that roots preferentially occupy extant pores (Dexter, 1987; White and Kirkegaard, 2010) versus perforating soils de novo, compacting soil in their immediate surroundings in the process (Helliwell et al., 2017; Martinez et al., 2021). Both outcomes have important implications for porosity, bulk density, and water flow (Lucas et al., 2019a; Lu et al., 2020; Sullivan et al., 2022). Thus, deep roots can control SOC at depth not only by the changes in direct C inputs, but also by influencing structural characteristics that define pore space and thus the ability of water to transport organic compounds down-profile.

Given that the distribution of roots through a soil profile can control SOC inputs to relatively deep soil layers (i.e., greater than the horizon in which root abundance is greatest) via diverse direct and indirect mechanisms, surface activities such as land-use change that alter a system's root abundances may exert influences more deeply in the profile than is typically appreciated (i.e., the plow layer). While direct effects of land-use conversion on soil C stocks have been extensively studied (Houghton, 1995; Post and Kwon, 2000; Guo and Gifford, 2002; Deng et al., 2016; Sulman et al., 2020; Beillouin et al., 2022), more recent investigations have begun to explore these influences in relatively deep horizons (Rumpel and Kögel-Knabner, 2011; Sulman et al., 2020). For instance, losses of deep roots via land-use change are known to alter deep soil biogeochemical environments even below the zone of highest root densities (Billings et al., 2018); this has important implications for the overall SOC stocks (Jobbágy and Jackson, 2000). However, the interacting effects of root abundances, soil moisture availability, and soil structure on SOC depth distributions are only rarely explored, especially considering changes to the landscape and climate promoted by anthropogenic activity.

We investigated the role of these ecosystem features on the depth distribution of SOC in the C-rich Mollisols of the upper U.S. Midwest. We used a dataset derived from the National Cooperative Soil Survey Soil Characterization database to parameterize and compare the rate of SOC decrease with depth under plowed and unplowed lands across a climatic gradient at a regional scale. To uncover the mechanisms driving these vertical SOC patterns in different land uses, we analyzed samples from soil profiles sampled over a smaller area representative of the same land use and climate gradient present in the larger dataset for biological, physical, and chemical characterization to 2 m depth. We hypothesized that greater availability of water in these systems promotes the growth and transport of living (i.e., roots) and dead surficial, in-situ C downprofile and that this downward flux both influences and is mediated by soil structural attributes which are, in part, governed by biotic activity. We test this hypothesis working across gradients of effective precipitation and land use, examining the relationships between SOC depth distributions, root abundances, soil radiocarbon signatures, aggregate size distribution, and soil microbial activity. Our work helps to clarify the pace at which human activities can modify soil structural and biotic characteristics in ways relevant for a soil's capacity to store C and promote ecosystem functions in a changing climate.

#### 2. Materials and methods

#### 2.1. Regional-scale patterns of SOC depth distributions: The PEDS dataset

We used a recently compiled dataset (the Pedogenic and Environmental DataSet; PEDS) from Koop et al. (2020) and Mohammed et al. (2020) to explore patterns of SOC depth distributions as influenced by water availability and land use across Mollisols of the U.S. Midwest. We focus on Mollisols given its wide distribution across the region of interest and the agricultural value of these soils. This dataset contains field-based, pedon-scale information and laboratory data collected through the United States Department of Agriculture Natural Resources Conservation Service (USDA-NRCS) National Cooperative Soil Survey (NCSS) and climate data from both the Parameter-elevation Regressions on Independent Slopes Model (PRISM; PRISM, 2021) and WorldClim 2 (Fick and Hijmans, 2017). We selected the profiles classified as Mollisols within the U.S. Midwest (i.e., the states of Illinois, Indiana, Iowa, Kansas, Michigan, Minnesota, Missouri, Nebraska, North Dakota, Ohio, South Dakota, and Wisconsin; U.S. Census Bureau, 2020).

Within this region, we extracted a total of 4,305 profiles for which SOC concentration data, in %, where available. From these, we excluded those that did not have mean annual precipitation (MAP) or potential evapotranspiration (PET) data (n = 58 excluded) with which we could calculate effective precipitation (EfP; see Section 2.2 for calculation of  $E_fP$ ) or did not have a measurement of SOC for the surficial horizon (n =175 additionally excluded). We also excluded profiles where O horizons were present because of their relatively low numbers (n = 18) and their disproportionate influence on surface horizon SOC model estimates (see below). Finally, we excluded profiles with fewer than four observations of SOC, which was the minimum number of observations needed with which to fit the exponential decay model used in this work. Agricultural soil profiles were defined as those with the presence of an Ap horizon; all other soil profiles were considered to have never been plowed (termed 'native prairie' systems). We used SOC concentration data for each soil layer and its known depth (here corresponding to the depth of the horizon thickness midpoint) from the remaining 2,941 soil profiles (2,158 and 783 profiles, and 14,573 and 4,806 horizons from agricultural and native prairie systems, respectively) to fit an exponential decay model of SOC concentration with depth (see Section 2.4.) separately for each pedon.

We calculated SOC stocks using SOC concentrations and bulk density data based on the horizon thickness for the 605 profiles in PEDS for which both of these data types were available. As for analyses leveraging SOC concentrations, we excluded profiles that did not have at least four observations of SOC stock (gC cm $_{\rm Soil}^3$ ) at different depths (n=92) and did not have a SOC stock calculated for surficial horizons (n=32) to fit the exponential decay model. Similar to what was done using SOC concentrations, we used the available SOC stock for each horizon and its known depth (i.e., the depth corresponding to the horizon thickness midpoint) from the 481 profiles across the US Midwest (375 and 106 profiles and 2,417 and 628 horizons from agricultural and native prairie systems) to fit an exponential decay model of SOC stocks with depth for each pedon. We compared model parameter estimates based on these depth distributions of SOC concentration and stocks to investigate the importance of bulk density to SOC depth distributions (see Section 2.6).

# 2.2. Discerning mechanisms driving regional-scale patterns of SOC depth distributions

### 2.2.1. Study sites and sampling methods

We ran a comprehensive set of soil analyses on soil samples from four precipitation regions in the state of Kansas collected from genetic horizons obtained from excavated soil pits of approximately two meters deep, under agricultural and native prairie systems, in collaboration with the Natural Resources Conservation Service (NRCS) on the dates shown in Table 1. From east to west, the Eastern Kansas (EKS), Konza

(KNZ), Hays (HAY), and Tribune (TRB) sites fall along a decreasing gradient of mean annual precipitation (MAP). Further information about the sites where excavated profiles were sampled, including soil series and historical climatic data, are displayed in Table 1. None of the agricultural sites sampled are irrigated (i.e., all are rain-fed).

Tribune is the westernmost site where soil profiles were excavated in the Kansas State University Southwest Research Center. The native prairie is composed of C3 and C4 grasses, where buffalo grass (*Bouteloua dactyloides*) is the dominant species. The agricultural site is characterized by a wheat-grain sorghum-fallow rotation with tillage and was sampled after wheat harvest.

Native prairie sites sampled in Hays consists of mixed-grass prairie, with a dominance of the C4 plants, such as little bluestem (*Schizachyrium scoparium*), Sideoats grama (*Bouteloua curtipendula*), and forbs, though C3 plants cuman ragweed (*Ambrosia psilostachya*) and purple prairie clover (*Dalea purpurea*) are also present (Heisler-White et al., 2009). The agricultural site was sampled at the Kansas State University Agricultural Research Center facility, which has been historically farmed as a wheat-sorghum-fallow rotation with minimum tillage during the fallow period.

The Konza sites were sampled at the Konza Prairie Biological Station. The native prairie site is dominated by perennial C4 grasses, such as big bluestem (*Andropogon gerardi*) and Indian grass (*Sorghastrum nutans*), and C3 herbaceous forb species (Heisler-White et al., 2009). Agricultural soils at this site have been cultivated with soybean, wheat, and grain sorghum since the 1960s with tillage and local fertilizer and pesticide application practices (Jangid et al., 2010).

The native prairie site in Eastern Kansas was sampled at the Welda Prairie (a part of the Anderson County Prairie Preserve near Welda, KS) is dominated by C4 grasses and C3 forbs (Kettle, 2016). The agricultural site was sampled 39.9 km away from the native prairie site in Ottawa, KS, at the Kansas State University East Central Experiment Field, where for the past 12 years there has been a crop rotation between corn and soybean.

We also sampled soils in twelve locations under agricultural and native prairie systems across the effective precipitation in Kansas, U.S. (Table 1) using a Giddings probe (Giddings Machine Company, USA) down to 150 cm whenever possible for the fixed depth intervals of 0–5, 5–15, 15–30, 30–75, and 75–120 or 150 cm, which we used to run a specific, less extensive set of analyses (see section 2.3). All collected samples were kept at  $-20\,^{\circ}\mathrm{C}$  after homogenization at the Kansas Biological Survey and Center for Ecological Research (KBS-CER) at the University of Kansas. Sampling dates, MAT, and MAP for these twelve locations are shown in Table 1. Though crops and thus fertilization practices differed across the agricultural plots at the time of sampling, we focus on two relatively durable characteristics broadly typical of annually-harvested, row-crop agriculture: declines in deep roots relative to native perennial systems, and altered soil structure.

The state of Kansas is characterized by a strong variability in climatic conditions across space and time that shape the distribution of the vegetation along the west-to-east transect (Rahmani and Harrington, 2019). We leverage effective precipitation ( $E_fP$ ) to gauge the effects of climate variability on the depth distribution of SOC.  $E_fP$  is a unitless value based on the ratio of potential evapotranspiration (PET) and MAP, where values equal or greater than 0 indicate that the evapotranspiration needs are met by MAP:

$$E_{f}P = 1 - \frac{PET}{MAP} \tag{1}$$

By reflecting the ecosystem's capacity to meet the evapotranspiration demands,  $E_fP$  is a proxy for water potentially available for soil processes after atmospheric demands are met. Although the  $E_fP$  concept is more commonly used to reflect the precipitation amount necessary to meet the potential transpiration needs of a cropped area (Bos et al., 2009), we use it in this study as an estimate of the net amount of water that can infiltrate soils (Marek et al., 2016).

 Table 1

 Study sites across the state of Kansas, USA. Site names in bold font represent sites where soils were subjected to a greater number of analyses (see text for detail).

Site	Land use	Latitude	Longitude	MAP <sup>1</sup> (mm)	MAT <sup>2</sup> (°C)	Date Sampled (YYYY- MM-DD)	Sampling Method	Soil series <sup>3</sup>	Parent material <sup>3</sup>	Slope <sup>3</sup>
Tribune, KS (TRB)	Agriculture	38°28′09″N	101°46′55″W	456	11.3	2019-08- 19 2019-11-	Giddings Genetic	Richfield	Loess	0–1%
	Native prairie	38°28′10″N	101°46′56″W	456	11.3	05 2019-08- 19 2019-11-	horizons Giddings Genetic	Richfield	Loess	0–1%
Logan County (LGN)	Native prairie	38°47′19″N	101°10′01″W	471	11.6	05 2021-07- 07	horizons Giddings	Ulysses	Loess	0–1%
Smoky Valley Ranch (SVR)	Agriculture	38°52′18″N	100°58′58″W	478	11.6	2019-07- 18	Giddings	Ulysses	Loess	0–1%
	Native prairie	38°51′57″N	100°59′42″W	476	11.7	2019-07- 18	Giddings	Ulysses	Loess	6–15%
Trego County (TRG)	Agriculture	39°00′48″N	99°45′37″W	580	12.0	2021-07- 08	Giddings	Penden	Loess over alluvium	1–3%
	Native prairie	39°00′54″N	99°44′40″W	580	12.0	2021-07- 08	Giddings	Holdrege	Loess	1–3%
K-State Agricultural Research Extension Facility (HAY)	Agriculture	38°50′34″N	99°18′52″W	604	12.3	2018-05- 08 2018-08-	Giddings Genetic	Harney	Calcareous loess	0–1%
Hays, KS (HAY)	Native prairie	38°50′07″N	99°18′11″W	604	12.3	23 2018-05- 08 2018-08-	horizons Giddings Genetic	Harney	Calcareous loess	0–1%
Rooks County (RKS)	Agriculture	39°14′30″N	99°12′52″W	627	11.8	23 2019-08-	horizons Giddings	Harney	Loess	0–1%
	Native prairie	39°10′29″N	99°09′00″W	638	11.9	26 2019-08- 26	Giddings	Harney	Calcareous loess	0–1%
Hanks Nature Conservation (HNC)	Agriculture	38°53′17″N	97°59′29″W	740	12.7	2021-08- 06	Giddings	Wells	Residuum weathered from sandstone and shale	3–7%
	Native prairie	38°53′31″N	97°59′15″W	740	12.7	2021-08- 06	Giddings	Wells	Residuum weathered from sandstone and shale	3–7%
The Land	Agriculture	38°41′39″N	97°35′28″W	780	13.2	2019-08- 26	Giddings	Hord	Alluvium	0–1%
Institute (TLI)	Native prairie	38°58′11″N	97°28′08″W	760	13.3	2019-08- 26	Giddings	Hord	Alluvium	0–1%
Konza Prairie	Agriculture	39°06′11″N	96°36′15″W	858	12.7	2018-05- 11	Giddings	Reading	Alluvium	0–2%
Biological Station (KNZ)	N	00006/10//	06006105///	056	10.7	2018-11- 08	Genetic horizons	D 1:		1 00/
	Native prairie	39°06′19″N	96°36′35″W	856	12.7	2018-05- 11 2018-11- 08	Giddings  Genetic  horizons	Reading	Alluvium	1–3%
Jefferson County (JEF)	Agriculture	39°20′04″N	95°30′27″W	964	12.8	2021-06- 23	Giddings	Sibleyville	Sandy and silty residuum weathered from sandstone and	3–7%
	Native	39°02′43″N	95°12′17″W	991	12.7	2021-06-	Giddings	Pawnee	shale Till	4–8%
	prairie					23	, and the second			
Leavenworth County (LVN)	Native prairie	39°15′31″N	94°58′42″W	1000	12.5	2019-09- 18	Giddings	Sharpsburg	Loess	1–4%
Ottawa, KS (EKS)	Agriculture	38°32′19″N	95°14′51″W	1009	13.0	2018-05- 17 2019-07-	Giddings Genetic	Woodson	Silty loess and/or silty and clayey alluvium	0–1%
Welda Prairie (EKS)	Native	38°10′52″N	95°16′20″W	1041	13.2	23 2018-05-	horizons Giddings	Olpe	Silty loess and/or	3–7%
	prairie					23 2019-04- 24	Genetic horizons		ancient clayey alluvium	

<sup>&</sup>lt;sup>1</sup>MAP: Mean annual precipitation; <sup>2</sup>MAT: Mean annual temperature; <sup>3</sup>Natural Resources Conservation Service (NRCS) Soil Survey data (https://websoilsurvey.sc.egov.usda.gov/).

#### 2.3. Soil analyses

#### 2.3.1. SOC concentrations

We measured total SOC concentration of all soil samples collected across the state of Kansas, regardless of sampling method (i.e., sampled from a pit face or via Giddings probe), by subsampling the soils stored at  $-20\,^{\circ}\text{C}$ . These subsamples were oven-dried at 60  $^{\circ}\text{C}$  for at least 48 h, had visible roots and rocks removed prior to being ground to a fine powder, and then were exposed to acid fumigation in a desiccator following Ramnarine et al. (2011) to remove carbonates. After fumigation, the samples were dried again at 60  $^{\circ}\text{C}$  for 24 h and sent to the Kansas State Stable Isotope Mass Spectrometry Laboratory for analysis of total SOC using the Elementar Vario PYRO cube (Elementar, Germany).

#### 2.3.2. Additional analyses of samples from excavated soil profiles

Samples collected by diagnostic horizon from the excavated soil profiles at most locations in Kansas (HAY, KNZ, and EKS; Table 1) went through an additional set of analyses (see Sections 2.3.2.1 to 2.3.2.3) aimed at investigating the drivers of SOC depth distribution across the climatic gradient in Kansas. Samples from the profiles excavated in Tribune, KS, were collected at a later date and did not go through this set of analyses.

2.3.2.1. Radiocarbon signatures of SOC. We leveraged radiocarbon signatures of SOC to explore the degree to which rooting abundance, location on the precipitation gradient, and soil structure influence inferred SOC persistence. To that end, another subsample of the soils stored at  $-20\,^{\circ}\text{C}$  was oven-dried at  $60\,^{\circ}\text{C}$  for over 48 h and had all visible roots and rocks removed prior to being manually ground to a fine powder. The samples were dried at  $60\,^{\circ}\text{C}$  again for 24 h and sent to the University of Georgia Center for Applied Isotope Studies for analysis. There, samples were subjected to hot acid washing to remove acid-soluble OC pools. Graphite targets were extracted from organic samples via combustion, cryogenically separated, and analyzed for isotopic signatures using the AMS system (Pelletron 0.5 mV 1.5DH-1, Cherkinsky et al., 2010; Cherkinsky et al., 2018). The fraction of modern C (FM) of the sample is reported based on the known <sup>14</sup>C content of an accepted standard (Trumbore, 2009).

2.3.2.2. Water-stable aggregate size distribution. To understand how changes in SOC inputs may affect soil aggregation, we characterized the water-stable aggregate size distribution following a modified procedure based on Nimmo and Perkins (2002) at the University of California—Riverside. We focus on intermediate aggregate sizes, capturing the majority of our soil sample mass. Our approach isolated aggregates smaller than 4.75 mm in diameter (defined by sieve mesh) and greater than 0.21 mm; aggregates smaller than the minimum diameter are lost during the separation process. Briefly, we used a modified Dickson apparatus (Dickson et al., 1991) to wet a known amount of air-dried soil sample by slow wicking. We note that the soil homogenization technique used upon soil collection removed larger clods, which were broken along planes of weakness prior to air-drying. When the sample was saturated, we transferred the soil onto a stack of sieves in a Yoder device, where sieves were raised and lowered in tap water at approximately 2.8 cm per stroke for 10 min, at a frequency of 36 S min<sup>-1</sup>. The samples were then oven-dried at 105 °C overnight and, after weighing, the soil in each sieve size was dispersed in a mixer with 2 g/L of sodium hexametaphosphate for 10 min. The dispersed sieved subsamples were passed through the same sieves and the remaining debris was dried prior to weighing. This step allowed us to distinguish true soil aggregates on each sieve from individual soil particles, rock and plant fragments that were larger than the sieve opening. We analyzed each sample in triplicate to obtain a more robust estimate of the average aggregate-size proportion for each horizon. The aggregate sizes were determined by the diameter of the sieves and divided into five intervals: <0.21 mm,

0.21–1 mm, 1–2 mm, 2–4.76 mm, and >4.76 mm. The results are reported as a proportion of the total soil sample. We calculated the geometric mean aggregate size for each interval,  $d_i$ , following Koop et al. (2020):

$$d_i = \exp\left[\frac{\ln(l_i) + \ln(u_i)}{2}\right] \tag{2}$$

where l represents the lower boundary and u the upper boundary of each aggregate size interval i. For the smallest aggregate size fraction, we used a lower boundary equal to the threshold of clay domains (i.e., 0.002 mm; Dexter, 1988; Six et al., 2004) to avoid the log of zero. Because the upper boundary was unknown for the largest aggregate size, we set the value of  $u_i$  to 4.76. Each value of d was used to calculate the geometric mean aggregate diameter (MAD) for each jth horizon (Koop et al., 2020) as follows:

$$MAD_{j} = \exp\left[\frac{\sum_{i=1}^{m} f_{i} \ln(d_{i})}{\sum_{i=1}^{m} f_{i}}\right]$$
(3)

where f is the volume fraction of the aggregate interval i, and m represents the number of aggregate intervals. Values of MAD are reported in mm.

To simplify some of our analyses, we also divided the five aggregate sizes into three aggregate classes, reported as a proportion to the total amount of soil. We refer to aggregates smaller than 0.21 mm in diameter as microaggregates. Aggregates between 0.21 and 4.76 mm in diameter were called intermediated-sized macroaggregates, as this class includes the lower threshold for characterization of macroaggregate sizes (0.25 mm; Ghezzehei, 2011) and has a defined upper size threshold set at 4. 76 mm. We refer to aggregates greater than 4.76 mm as large macroaggregates, a category that does not have an upper size threshold with our sieve selection.

2.3.2.3. Salt-extractable organic carbon (EOC) concentrations. To explore the relative contribution of rooting systems to the concentrations of organic acids in solution, we first quantified the EOC by extracting the soils stored at -20 °C using a salt solution. Specifically, we subsampled 10 g of field-moist sample into a 50 mL Falcon tube and added 40 mL of 0.5 mol K<sub>2</sub>SO<sub>4</sub>, placed it on a platform shaker at 200 rpm for one hour, and centrifuged and filtered the resulting suspension using a 0.45 µm syringe filter. The concentration of EOC in the extracts was determined by colorimetry as described by Bartlett and Ross (1988) and analyzed in a Synergy HT microplate reader (Agilent, USA). We normalized the EOC concentrations by the averaged total root abundances of the same soil layer (i.e., including fine and coarse roots; see Section 2.4 for characterization of rooting abundances). Not all EOC is root-derived, but this metric allows us to probe soil horizons where concentrations of root and microbial exudates such as organic acids (Herbert and Bertsch, 2006) may reflect greater or lesser connection to roots. For simplicity, we refer to this metric as EOC per unit of total root abundance.

#### 2.4. Photo-derived root densities

For the eight sites where soil profiles were excavated (Table 1), we cleaned the pit face along natural planes of weakness and generated high resolution photos along the length of the pit face. We used these photos to obtain photo-derived fine and coarse root abundances down to two meters under native prairie and agricultural systems as described in Billings et al. (2018) and Hauser et al. (2020). Briefly, a 1x1 cm grid was overlaid on the photos and the presence or absence of roots was recorded. Fine roots had diameter <1 mm, and all diameter sizes equal to or greater than 1 were considered coarse roots. We counted each photo grid cell where roots were present in 1-cm depth increments, and divided by the width of the analyzed soil profile. Absolute root abundances for each depth increment z are given as:

Root abundance 
$$z(absolute) = \frac{\sum cells \text{ with presence of roots}_z}{\sum total cells analyzed_z}$$
 (4)

We used this dataset to explore the changes in rooting depth distributions with land-use conversion across the climatic gradient in Kansas. We also report normalized root abundances for each depth increment z, calculated as:

Root abundance 
$$z_{\text{(normalized)}} = \frac{\sum \text{cells with presence of roots}_z}{\sum \text{cells with presence of roots}_p} *100$$
 (5)

where the numerator is the sum of all roots present at each depth increment, z, and the denominator is the sum of all roots present in the profile, p. We calculated both absolute and normalized root abundances for fine and coarse roots separately.

#### 2.5. Fitting exponential decay models

The SOC decline with depth has been the subject of many studies (Jobbágy and Jackson, 2000; Lorenz and Lal, 2005; Minasny et al., 2006; Mishra et al., 2009; Sulman et al., 2020; Sun et al., 2020; Franzluebbers, 2021) and can be expressed as an exponential decay function:

$$SOC_z = SOC_f + (SOC_i - SOC_f)e^{(-\beta^*z)} + \varepsilon$$
 Eq. (6)

where  $SOC_z$  corresponds to the SOC either as concentration (%) or stock (gC cm<sup>-3</sup>) at depth z (cm), SOC<sub>i</sub> is the predicted SOC at the surface (depth = 0 cm), SOC<sub>f</sub> is the lowest predicted SOC value of the profile,  $\beta$  is the rate of SOC decrease with depth, and  $\varepsilon$  is the error term. We fit this function using SOC concentrations at their corresponding depths (SOC<sub>z</sub> and z) of soil profiles in PEDS wherever we had data available, and for all sampled profiles across Kansas, to obtain  $SOC_f$ ,  $SOC_i$ , and  $\beta$  values. We estimated the parameters using the Nelder-Mead simplex algorithm to minimize the residual error, which is a direct search method often applied to nonlinear regressions for optimization (Nelder and Mead, 1965). We also applied this methodology to a subset of the PEDS profiles for which bulk density observations (in gC cm<sub>soil</sub>) were available to fit this function to SOC stocks and evaluate if SOC depth distributions are better described by stocks compared to concentrations. We employed the coefficient of determination, R<sup>2</sup>, as a goodness-of-fit metric for the modeled SOC depth distributions and only selected profiles with R<sup>2</sup> greater than or equal to 0.8. We chose this value as the threshold to avoid an overconservative approach that would unnecessarily reduce the number of profiles for the statistical analysis, as approximately 10% of the fitted distributions, for both SOC concentrations and stocks, had R<sup>2</sup> between 0.8 and 0.9.

We used model estimates of  $\beta$  to evaluate how well-distributed SOC is with depth. Greater values of  $\beta$  indicate that SOC is concentrated closer to the surface and exhibits a relatively sharp decrease with depth; smaller values indicate more well-distributed SOC throughout the soil profile and a smoother, less abrupt decrease in C with depth (Minasny et al., 2006).

We used the fitted parameter estimates of  $SOC_f$ ,  $SOC_i$ , and  $\beta$  to predict SOC depth-distributions for each profile at 1-cm increments down to 500 cm. This approach allowed us to estimate the depth at which predicted SOC becomes indistinguishable from the predicted  $SOC_f$ . We considered values of modeled SOC estimates at 1-cm increments and  $SOC_f$  to be equivalent when their values matched to the fourth decimal place, and termed the depth at which this occurred as  $z_{SOC}$ .

### 2.6. Statistical analyses

We used log-transformed estimates of  $\beta$  to evaluate the effects of  $E_fP$  and land use on SOC depth distribution using linear models. We used the non-parametric linear model approach of quantile regressions (quantreg; Koenker, 2021) for the  $\beta$  values estimated from PEDS because model residuals could not be transformed to meet the assumptions of normality

and homoscedasticity. We do not report a conventional  $R^2$  statistic for these models as it is a product of least squares regression and are not applicable to nonparametric regressions. We instead report the nonparametric Spearman correlation,  $\rho$  (stats; R Core Team, 2022). Moreover, we assessed the correlation between the  $\beta$  values estimated from SOC concentrations and stocks also using the Spearman correlation. The depth-dependency of data points in many soil-related regressions is important to consider when selecting appropriate statistical models, but here we use these correlations only to assess the similarity of these model predictions. We used parametric linear regressions (stats; R Core Team, 2022) to evaluate the effects of  $E_f P$  and land use on estimates of  $\beta$  across Kansas.

Distributions of z<sub>SOC</sub> based on either SOC concentrations or SOC stocks calculated from PEDS were tested for different means under agricultural versus native prairie sites via a resampling-based test. Standard t-tests could not be used because the distributions of z<sub>SOC</sub> were not normally distributed. Although the t-test is fairly robust to departures from normality as long as distributions are still symmetric, the  $z_{SOC}$  distributions were also non-symmetric. Given n points  $x_1, ..., x_n$ and m points  $y_1, ..., y_m$ , from the two distributions, the resampling-based test resamples, with replacement, n points from the set  $x_1, ..., x_n$ , and m points from the set  $y_1, ..., y_m$ , and recomputes the difference between the means of the two resampled datasets. This procedure was repeated 10,000 times, and the difference between the means of the actual data was deemed significant if at least 95% (i.e., 9,500) of the resamplingbased values had the same sign as the difference-of-means computed on the real data. Nonnormal distributions and unequal variances prevented appropriate usage of traditional statistical approaches in which we could explore the effects of E<sub>f</sub>P at a larger scale.

For the SOC depth distributions across Kansas, we employed linear regression to evaluate the effects of both land use and  $E_tP$  on the  $z_{SOC}$  estimates. Inadequate spatial replication of multiple land uses at each of the three main soil sampling locations in Kansas prevented us from implementing traditional statistical analyses to evaluate the effects of the  $E_tP$  gradient and land use conversion on rooting depth-distributions, radiocarbon signatures, and water-stable aggregate sizes. Instead, we employed a regression approach on the SOC data collected in the field, leveraging the twelve sites across the Kansas precipitation gradient where we sampled native prairie systems and the ten sites across the gradients where we sampled cultivated lands (Table 1). All statistical analyses were performed using R v. 4.2.1 (R Core Team, 2022) and the results were considered significant when p < 0.05.

#### 3. Results

### 3.1. Modeling SOC depth distributions at the regional scale

We fit an exponential decay model to empirical depth distributions of SOC concentration based on the data available in PEDS (example profiles in Fig. S1) and used the resulting parameter estimates to assess the effects of water availability and native prairie conversion to agriculture on the SOC depth trends. Smaller estimates of  $\beta$  reflect more homogeneous distribution of SOC across depth, as demonstrated by model predictions down to 500 cm (Fig. 1a). Of the 2,941 profiles fitted by the exponential decay model, we selected only those where the minimum R<sup>2</sup> threshold was met, which eliminated 324 profiles (Fig. 2a). Another 11 profiles estimated  $\beta$  to be greater than 1000, which we also excluded from the statistical analyses. These relatively few pedons have the minimum number of observations necessary to fit the model but most SOC observations in each profile are zero, explaining overestimated  $\boldsymbol{\beta}$ values. We thus used model estimates for 2,606 profiles fitted with SOC concentrations for statistical analyses. Log-transformed values of  $\boldsymbol{\beta}$ estimated from SOC concentrations were significantly influenced by the interaction between  $E_fP$  and land use (Fig. 2b, 2c; p < 0.001) as evaluated by quantile regression, such that the slope of these values across  $E_{\mathrm{f}}P$ for agricultural soils was  $0.084 \pm 0.021 \text{ cm}^{-1}$  (p < 0.001) and for native

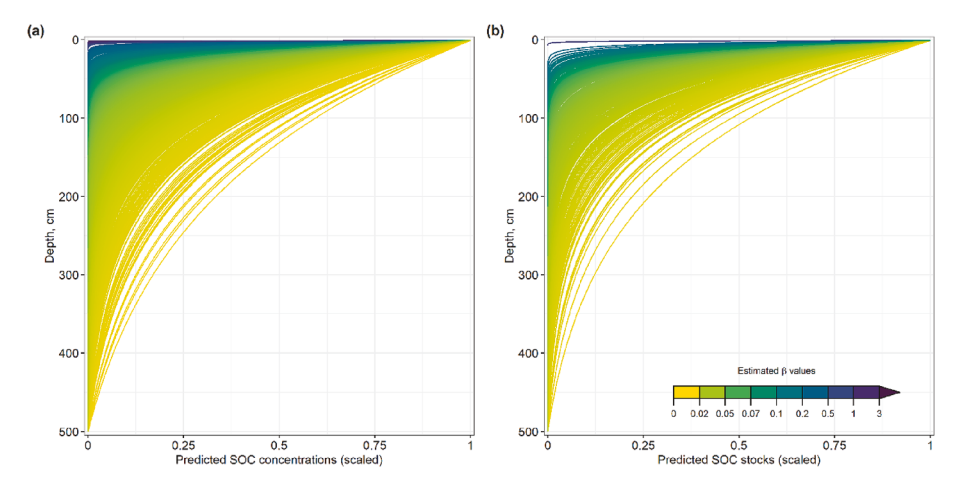


Fig. 1. Scaled predictions of SOC depth distributions down to 500 cm using the modeled exponential decay fits of SOC data in the PEDS database using SOC concentrations (a) and SOC stocks (b). Data displayed reflect the region described in text; we scaled the data by calculating the fraction of the total SOC in the profile present in each 1-cm depth increment to permit comparison of widely variable SOC values across 2,606 profiles.

prairie soils was  $-0.245 \pm 0.030 \text{ cm}^{-1}$  (p < 0.001).

We also fit an exponential model using SOC stocks calculated based on SOC concentrations and bulk density data for the 481 pedons in PEDS for which these data were available, of which 455 profiles met the  $R^2$  threshold criteria (Fig. 3a). The depth distribution of SOC stocks (Fig. 1b) yielded similar patterns than as those observed for SOC concentrations (Fig. 1a). Results for the log-transformed values of  $\beta$  using SOC stocks were significantly influenced by the interaction between  $E_fP$  and land uses (Fig. 3b, 3c; p<0.001) as evaluated by quantile regression. The relationship between  $E_fP$  and  $\beta$  exhibited a significant slope in native prairie soils, estimated as  $-0.257\pm0.074$  cm $^{-1}$  (p<0.001). The analogous slope for agricultural soils was non-significant (0.080  $\pm$ 0.043 cm $^{-1}$ ; p=0.066).

We evaluated the correlation between the predicted  $\beta$  from SOC concentrations and stocks for the 445 pedons where both parameters were available and the fit of the model was satisfactory, i.e., when the minimum  $R^2$  threshold was met. Using Spearman correlation, we observed a strong relationship between the two estimates ( $\rho_s = 0.926, p < 0.001$ ; Fig. 4a). We further demonstrated the similarity of the depth distributions of SOC concentrations and stocks using two exemplar profiles from PEDS in agricultural (Fig. 4b) and native soils (Fig. 4c) from which we estimated the  $\beta$  values.

Using the results from the exponential fits, we predicted the SOC depth-distributions by 1 cm increment down to 500 cm for all profiles across the US Midwest (Fig. 1; Fig. S1). That approach allowed us to calculate  $z_{\rm SOC}$  for all profiles (see Section 2.5.; Fig. 5). We observed deeper depths for  $z_{\rm SOC}$  estimates under agriculture (mean\_concentration = 399.2 cm; mean\_stock = 403.7 cm) regardless of whether we used SOC concentration or stocks compared to native sites (mean\_concentration = 344.3 cm; mean\_stock = 340.7 cm). Results from the resampling-based test confirmed that  $z_{\rm SOC}$  is significantly different under these two land uses using either SOC concentrations or stocks (p < 0.001 for both analyses).

#### 3.2. SOC depth-distributions at a local scale across Kansas

To discern the mechanisms driving the regional-scale relationships of SOC depth distributions, we obtained detailed soil biological, chemical, and structural data at a smaller scale using the data from 12 native prairie and 10 agricultural Mollisol profiles sampled across Kansas (Fig. 6a). In two instances, we removed one SOC concentration observation from two profiles at depths between 50 and 150 cm that were obvious excursions from the otherwise smooth exponential decline in SOC with depth. For the agricultural profile at the Konza Prairie Biological Station (KNZ), we elected to use SOC concentration data only from the genetic horizons to promote a more robust model estimation.

These corrections were necessary to better distinguish patterns of SOC depth distribution and do not affect the outcome of interest (the  $\beta$  estimates) as predictions of absolute SOC values are outside the scope of this paper. We assessed whether these well-characterized Kansan Mollisols exhibited similar patterns of  $\beta$  with  $E_fP$  as in the selected PEDS profiles, calculated using their SOC concentrations (Fig. S1). As observed in the native prairie PEDS Mollisol pedons, the Kansas sites exhibited significant, negative relationships between log-transformed  $\beta$  and E<sub>f</sub>P (p < 0.001), which were evaluated using linear regressions (Fig. 6b). Unlike in the PEDS profiles, slopes of agricultural and native prairie soils were both negative (-0.937  $\pm$  0.252 cm<sup>-1</sup>, and -1.017  $\pm$  0.184 cm<sup>-1</sup>, respectively), but native prairie soil values of log-transformed  $\beta$  were well-predicted by  $E_fP$  ( $R^2=0.93$ ) while agricultural soils exhibited a much looser fit ( $R^2 = 0.49$ ). The significant relationship between the logtransformed  $\beta$  and  $E_fP$  under agriculture falters when the value at the driest site sampled in Kansas is removed (Fig. 6b), which also improves the fit of the model ( $R^2 = 0.74$ ).

Similar to PEDS, we predicted SOC depth-distributions by 1-cm increment down to 500 cm using the results from the exponential fit for the profiles across Kansas (Fig. S1) and calculated the depth at which SOC concentrations become constant,  $z_{\rm SOC}$ . We leveraged the normality of the data collected across Kansas to evaluate the effects of  $E_{\rm f}P$  and land use on  $z_{\rm SOC}$  and found a significant relationship between  $z_{\rm SOC}$  and  $E_{\rm f}P$  in Kansans soils for native prairie sites (p=0.013) and for cultivated lands (p=0.014), though the fit of the model for the agricultural data was again looser than that from native prairie sites ( $R^2=0.331$  and  $R^2=0.818$ , respectively; Fig. 6c). The interaction between land uses across the  $E_{\rm f}P$  gradient is not significant for  $z_{\rm SOC}$  (p=0.573).

## 3.2.1. Root densities

The photo-derived root densities show an increase in the overall root abundance as  $E_fP$  increases under native sites, mostly driven by the increase in fine root abundances with greater water availability (Fig. 7b). Although the same increase is not realized under agricultural lands, greater absolute fine root abundances are observed outside the precipitation extremes (Fig. 7a). When considering the proportion invested in roots per cm of soil by the total rooting system, agricultural sites show greater variation in fine root investment (Fig. 7c) in comparison to the trends observed under most native prairie systems (Fig. 7d). Moreover, it appears that most sites invest similarly in fine roots abundance with depth across the  $E_fP$  gradient, except the site at the lowest  $E_fP$  extreme (Fig. 7d). Such a trend is not observed to the same degree for coarse roots because under agriculture these are almost non-existent except at shallow depths (Fig. 8a, 8c), and native prairie systems seem to invest more in this type of root where water availability is greater (Fig. 8b, 8d).

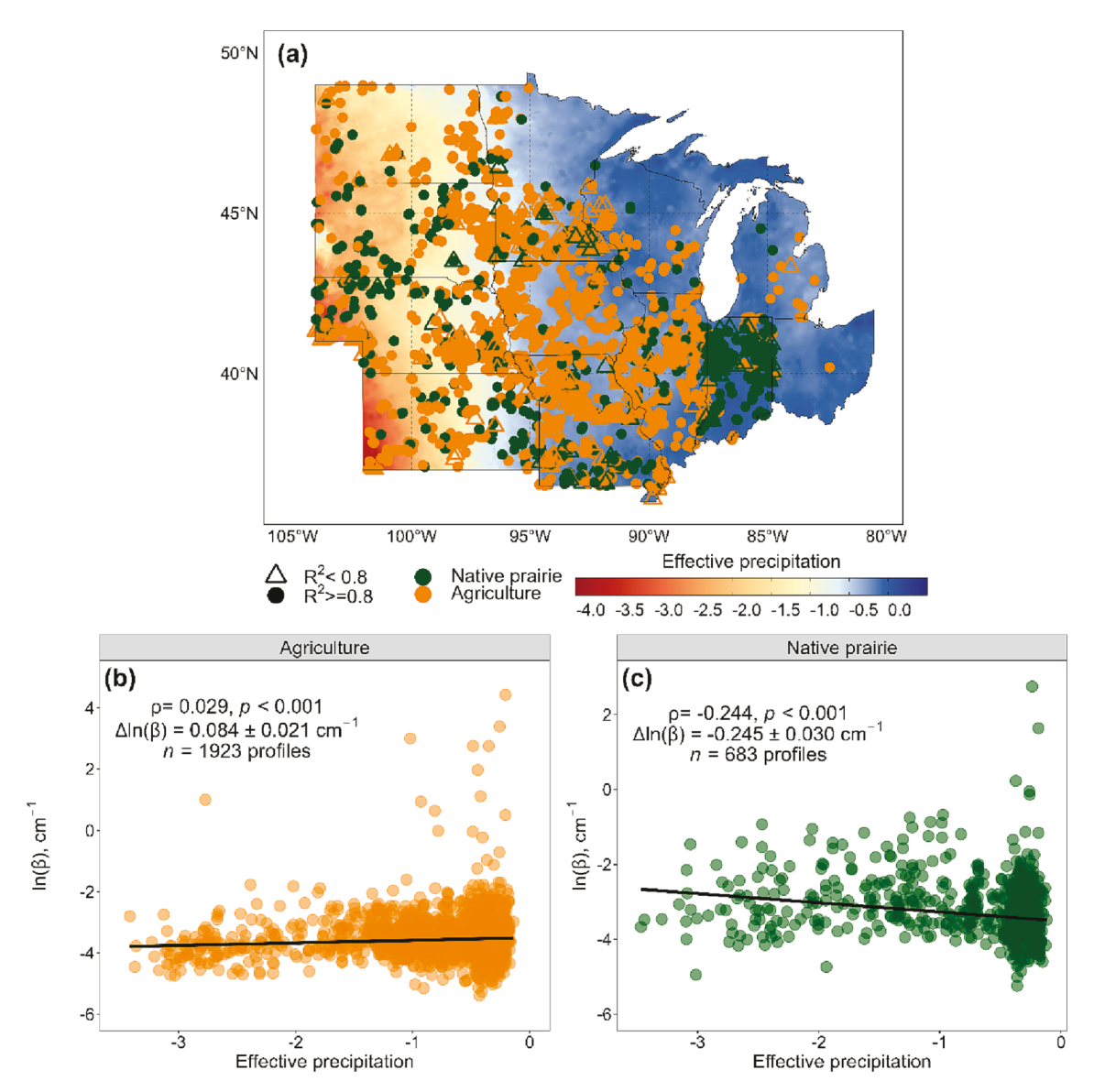


Fig. 2. Pedon locations and relationships between effective precipitation ( $E_fP$ ) and the parameter estimate describing the exponential decay of SOC concentrations with depth,  $ln(\beta)$ , derived from the PEDS dataset. (a) Map of selected Mollisol pedons available in PEDS fitted to an exponential decay model describing how SOC concentrations decline with depth. We used the  $R^2$  of each modeled pedon as a goodness-of-fit metric and established 0.8 as the minimum threshold for selection in statistical analyses (see text for detail). Closed points represent the profiles with  $R^2$  greater than or equal to 0.8, and open triangles represent profiles with  $R^2$  smaller than 0.8. Spatial representation of  $E_fP$  is based on precipitation data from PRISM (PRISM, 2021) and evapotranspiration data from Trabucco and Zomer (2018). (b and c) Parameter β from the model fit for the US Midwest profiles as it varies with effective precipitation for agricultural and native prairie sites, respectively. Statistics in (b) and (c) correspond to the Spearman correlation,  $\rho$ , the p-value and the slope,  $\Delta ln(\beta)$ , estimated from the quantile regression, and the n number of β estimates analyzed.

#### 3.2.2. Rooting activity

Normalizing the EOC concentrations by total root abundances in the soil profiles across Kansas displayed greater values with increased  $E_fP$  in both land uses (Fig. 9). There is a steady decrease in the normalized EOC under native prairie with depth (Fig. 9b), while agricultural lands showed an increase down to depths closer to 60 cm, then followed by a decrease (Fig. 9a). Particularly at the bottom of the measured soil profiles, we observed greater EOC in solution per unit total root abundance across depths in the agricultural soils at the wettest site.

#### 3.2.3. Radiocarbon

Radiocarbon signatures for six soil profiles across Kansas reveal generally greater abundance of FM (i.e., shorter transit times, Sierra et al., 2017) with greater  $E_fP$  (Fig. 10). Although native prairie soils generally have greater FM values at surface in comparison to

agricultural soils, deep soils in cultivated lands present greater FM than under native prairie.

#### 3.2.4. Soil aggregate-size distribution characterization

From the water-stable aggregate-size distribution analysis, we obtained the proportion of five aggregate sizes for each sampled horizon of six profiles in Kansas (Fig. S2). Because of inadequate field site replication, it was not possible to obtain standard deviations for the calculated metrics based on the aggregate-size distribution results. Using the calculated mean aggregate diameter per horizon (Fig. 11a, 11b), we observed the apparent breakdown of relatively large aggregates at the soil surface that typically occurs with plowing when compared to the native prairie (Six et al., 2000; Six and Paustian, 2014).

We normalized the proportion of the isolated soil aggregates by OC concentration (Fig. 11c, 11d) to investigate the propensity of bulk SOC

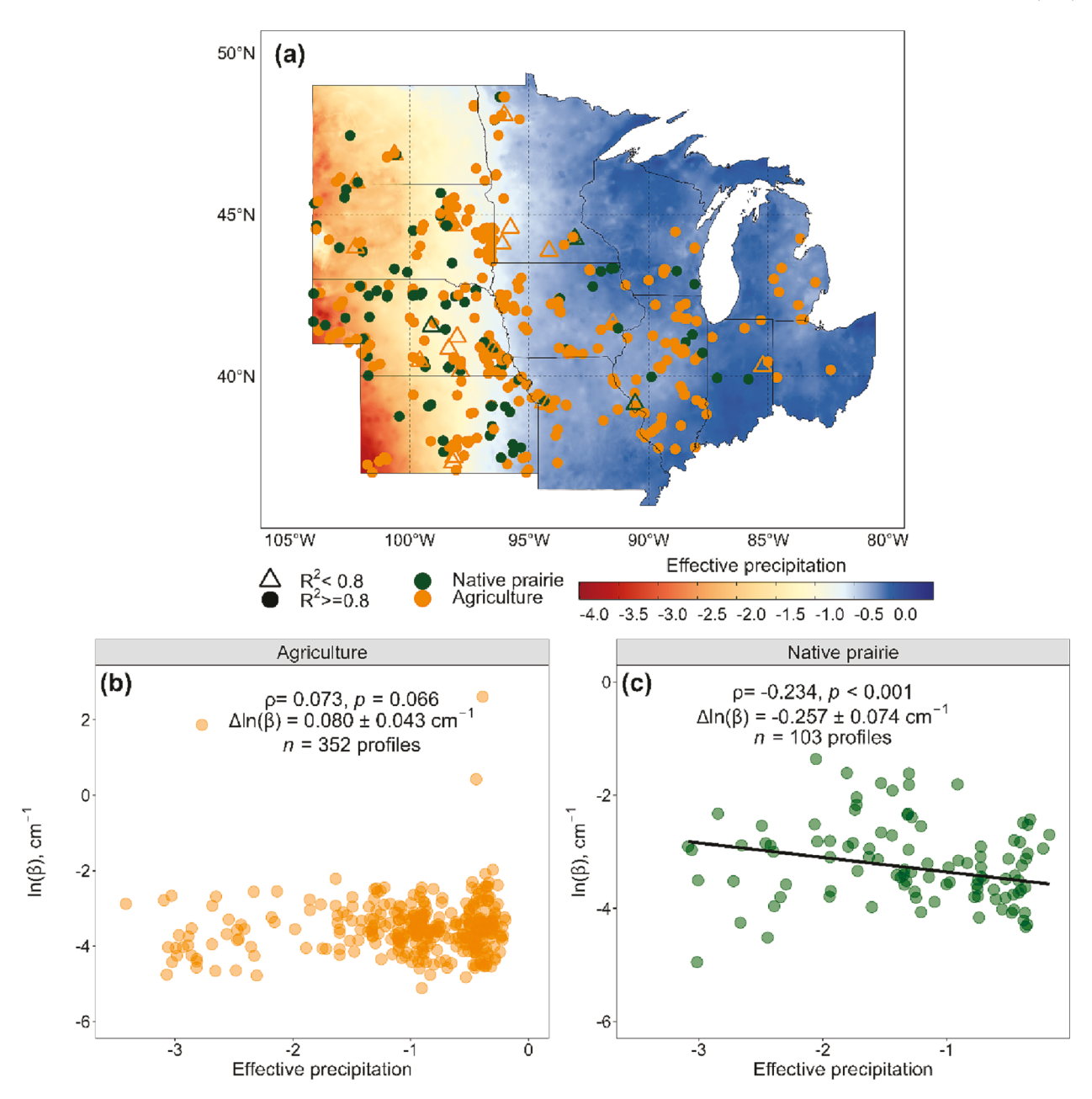


Fig. 3. Pedon locations and relationships between effective precipitation and parameter estimate describing the exponential decay of SOC stocks with depth,  $ln(\beta)$ , derived from the PEDS dataset. (a) Map of selected Mollisol profiles available in PEDS fitted to an exponential decay model describing how SOC stocks decline with depth. We used the  $R^2$  of each modeled pedon as a goodness-of-fit metric and established 0.8 as the minimum threshold for selection in statistical analyses (see text for detail). Closed points represent the profiles with  $R^2$  greater than or equal to 0.8, and open triangles represent profiles with  $R^2$  smaller than 0.8. Spatial representation of  $E_tP$  is based on precipitation data from PRISM (PRISM, 2021) and evapotranspiration data from Trabucco and Zomer (2018). (b and c) Parameter β from the model fit for the US Midwest profiles as it varies with effective precipitation for agricultural and native prairie sites, respectively. Statistics in (b) and (c) correspond to the Spearman correlation,  $\rho$ , the p-value and the slope,  $\Delta ln(\beta)$ , estimated from the quantile regression, and the n number of β estimates analyzed.

to form these aggregate sizes. We observed that the propensity of SOC to form and maintain these intermediate-sized macroaggregates is modified with land conversion. Specifically, greater  $E_{\rm f}P$  appears to promote the ability of SOC to form or protect intermediate-sized aggregates at depths greater than 100 cm in native prairie soils (Fig. 11c) while the opposite is observed in cultivated profiles around and below the same depth threshold (Fig. 11a).

#### 4. Discussion

Our work highlights the importance of investigating the depth to which climate and land conversion interact to affect SOC concentrations

and stocks throughout soil profiles, and the soil chemical, physical, and biological mechanisms that can drive these effects. We investigate the combined effects of water availability and conversion of native prairie to cultivated lands on SOC concentrations for Mollisols in the US Midwest, demonstrate the correspondence of these patterns with those for a smaller dataset of SOC stocks, and explore the roles of moisture availability, roots, and soil structure as mechanisms governing these processes across a relevant climatic gradient within Kansas, USA. Our findings have implications for understanding the capacity of soils to store persistent SOC and management strategies to promote SOC preservation for different land use systems considering the expected changes in precipitation patters under climate change.

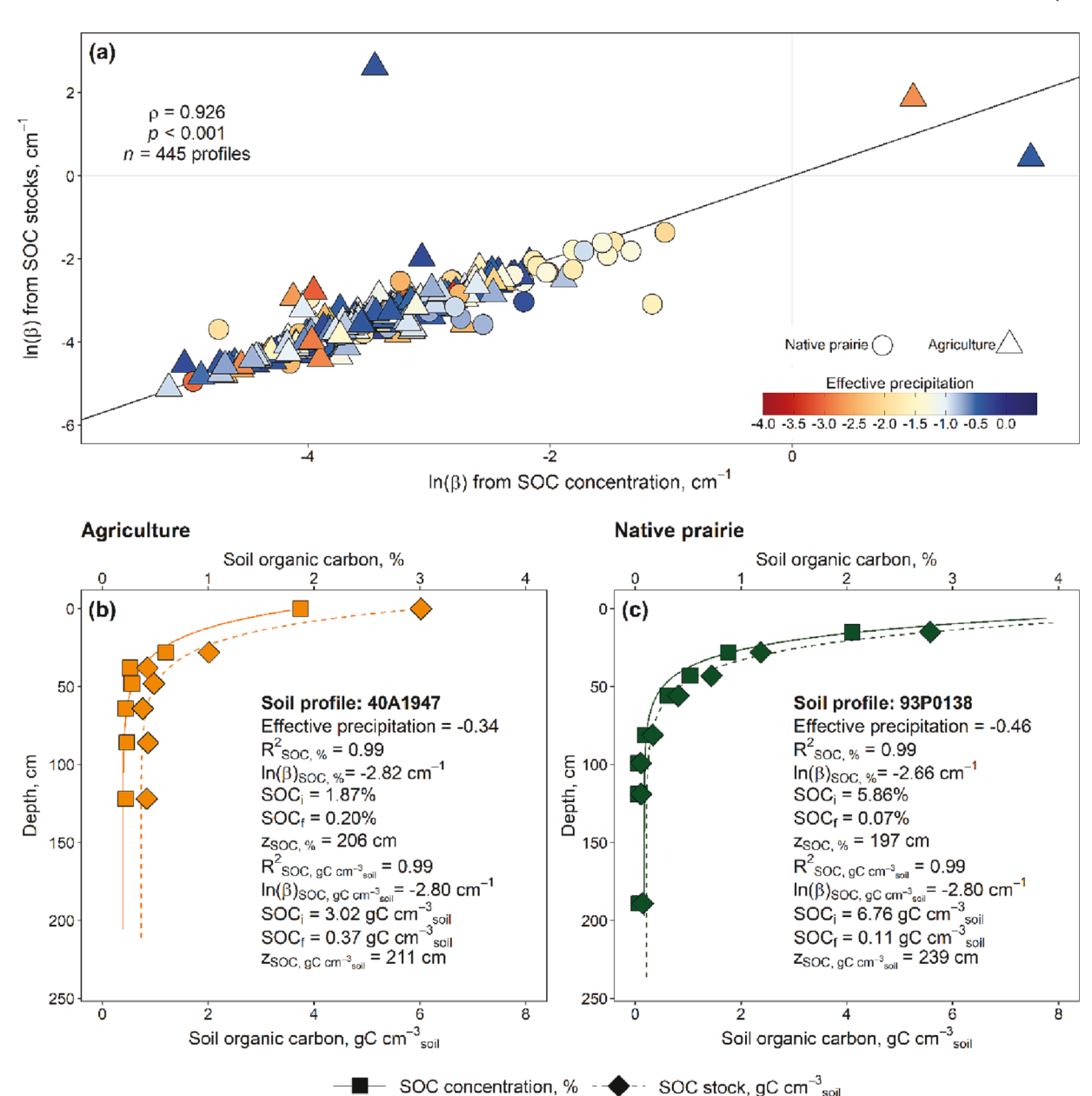


Fig. 4. Relationship of log-transformed values of the parameter  $\beta$  obtained from depth distributions of SOC concentrations with those derived from SOC stocks from PEDS (a). Exemplar comparisons of depth distributions of SOC concentration (%) and calculated SOC stocks (gC cm $^{-3}$ ) for an agricultural (b) and native prairie (c) profile from PEDS. In (b) and (c), solid lines represent the predicted depth distribution of SOC concentrations and dashed lines represent the predicted depth distribution of SOC stocks. Both (b) and (c) display estimated parameters for each curve.

## 4.1. SOC depth distributions across an effective precipitation gradient

The finding of a decrease in the rate of SOC decline with depth in native prairie soils with increased water availability (i.e., less negative values of  $E_f P$ ) across the upper US Midwest (Fig. 2c) suggests that greater  $E_f P$  promotes greater coupling among surficial and deeper horizons in native prairie soils, which is consistent with our hypothesis. We observed similar trends at the pedon scale across the precipitation gradient in Kansas, USA (Fig. 6b). These results allow us to draw parallels about the interplay of multiple mechanisms likely governing the SOC depth distribution across scales for these C-rich Mollisols, and can inform about these soils' varying capacity to transport and protect C under different management practices.

First, greater water availability promotes greater net primary productivity (NPP) in both natural and agricultural systems in the US Midwest (Twine et al., 2004; Motew and Kucharik, 2013), and we might

expect greater root inputs at any given depth in a system with greater NPP (Kleidon and Heimann, 1998; Kleidon and Heimann, 1998; Jackson et al., 2000). In addition to being a direct source of C to the soil, rooting systems can promote greater inputs of DOC via exudates into the rhizosphere (Pausch and Kuzyakov, 2018; Sokol et al., 2019), as suggested by the concentrations of EOC (see Section 4.2; Fig. S3). Such exudates likely can promote mineral-associated SOC given that rhizodeposits appear to be a more effective mechanism for C stabilization than OM derived aboveground (Sokol and Bradford, 2019). Therefore, as roots deepen into the soil, these processes can play an important role in enhancing the soils' ability to protect C with depth. In our study, a decrease in  $\beta$  (i.e., a less steep decline in SOC; Fig. 6b) is indeed accompanied by an increase in rooting abundances under native prairie systems (Fig. 7b, 8b).

As roots perforate into soils, they also can create new, and reinforce existing, biopores through which surficial C can flow downward

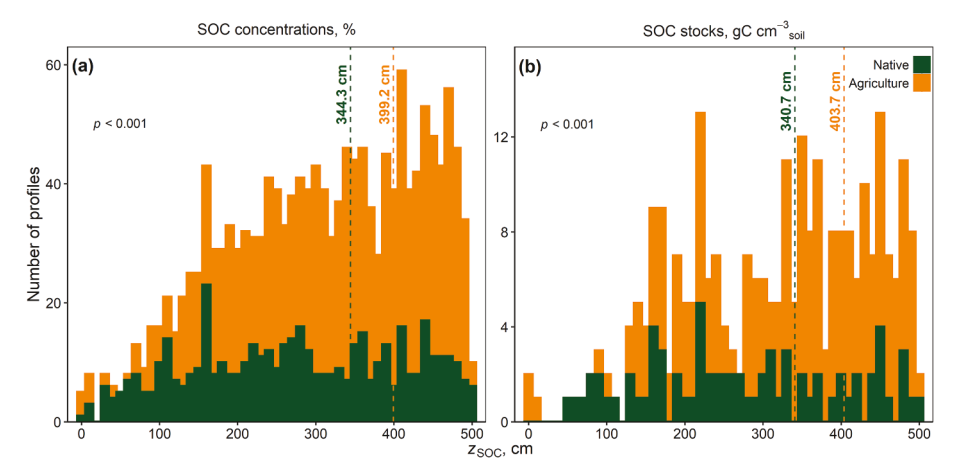


Fig. 5. Distribution of the depths at which SOC becomes indistinguishable from the predicted SOC<sub>b</sub> termed z<sub>SOC</sub>, for all PEDS profiles for which the exponential model was fitted and met the goodnessof-fit criteria. The  $z_{SOC}\ term\ thus\ represents the$ depth at which SOC becomes constant. Data displayed are estimates calculated using SOC concentrations (a) and SOC stocks (b). Dashed lines represent the average z<sub>SOC</sub> for each land use. For agricultural plots, 839 and 153 profiles exhibited values of  $z_{SOC}$  equal to 500 cm when calculated using SOC concentrations and SOC stocks, respectively; 208 and 30 profiles exhibited z<sub>SOC</sub> equal to 500 cm when calculated using SOC concentrations and stocks, respectively. Y-axis values are truncated below these values to permit visualization of patterns at lower values.

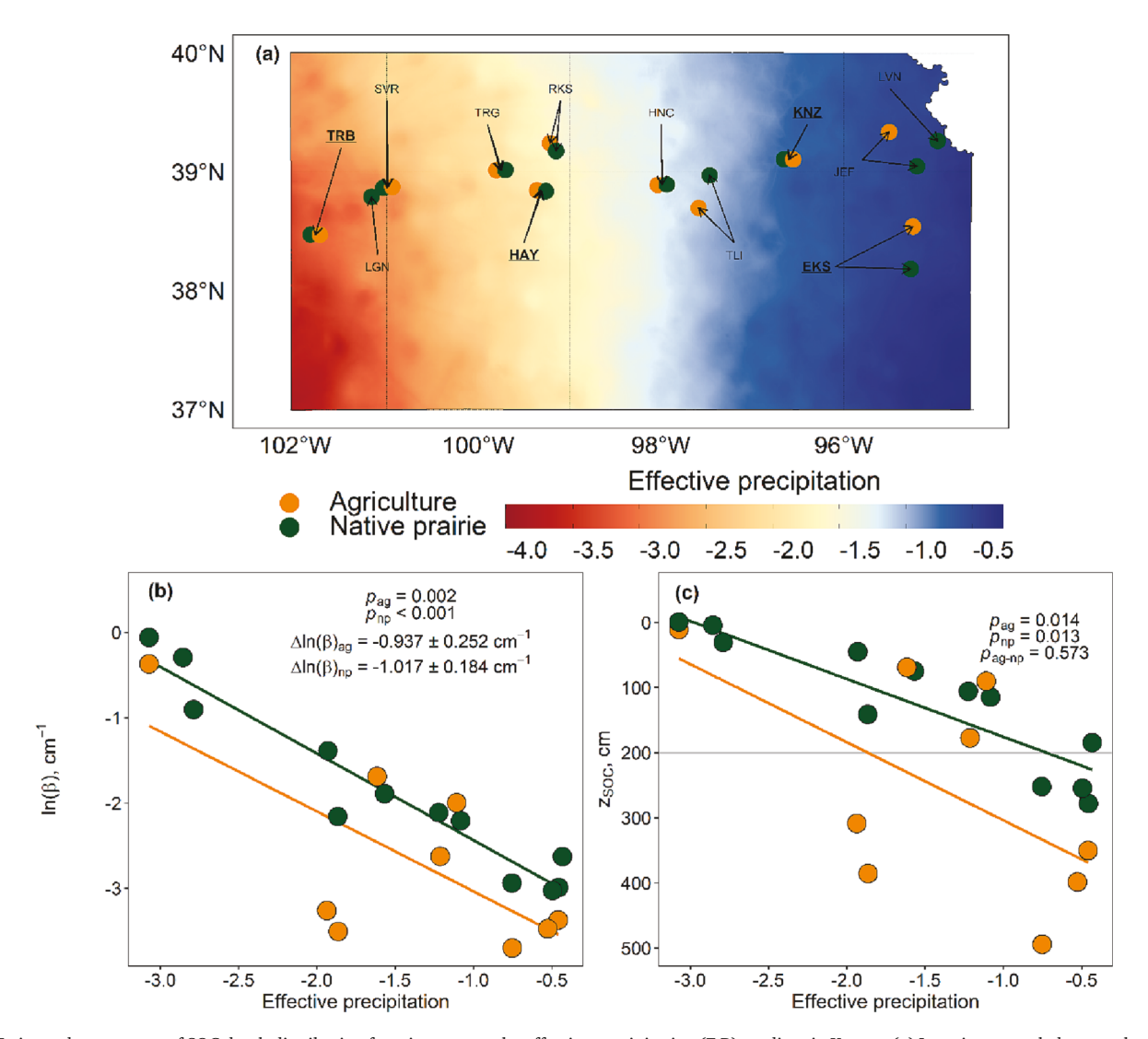


Fig. 6. Estimated parameters of SOC depth distribution functions across the effective precipitation ( $E_tP$ ) gradient in Kansas. (a) Locations sampled across the effective precipitation gradient in Kansas, USA. Site abbreviations represent locations sampled with a Giddings probe (Giddings Machine Company, USA). Underlined site abbreviations indicate locations additionally sampled for genetic horizons. See Table 1 for complete site names and information. Spatial representation of  $E_tP$  is based on precipitation data from PRISM (PRISM, 2021) and evapotranspiration data from Trabucco and Zomer (2018). (b) Log-transformed metric defining SOC decrease with depth,  $\beta$  as it varies with effective precipitation. (c) Estimated depth at which SOC becomes constant,  $z_{SOC}$ , as it varies with effective precipitation. See text for details of effective precipitation estimates. ag corresponds to statistics for the agricultural data. np corresponds to statistics for native prairie data.

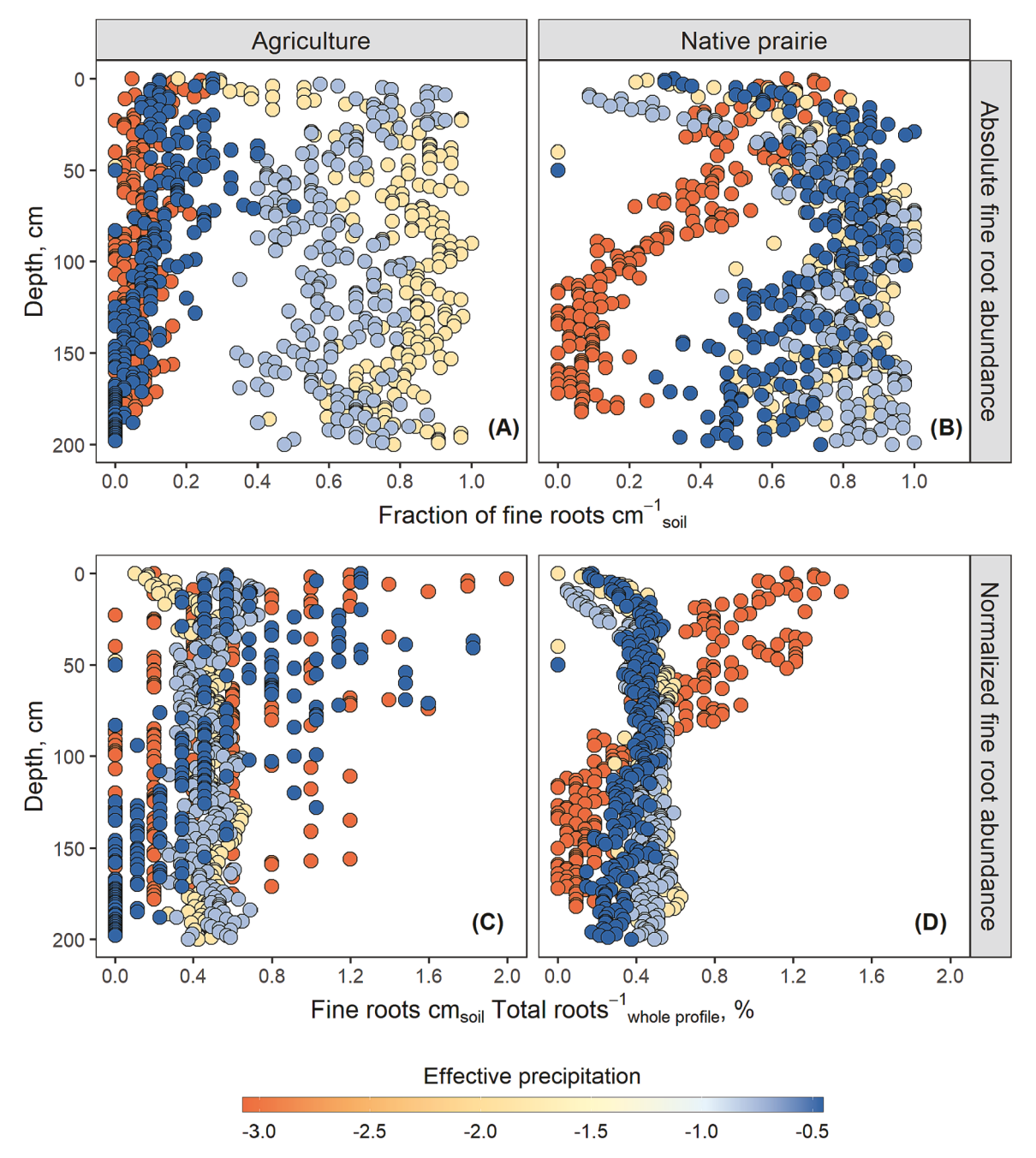


Fig. 7. Fine rooting depth-distributions across Kansas, USA. Results in (a, b) refer to the absolute root abundance, shown as a fraction of the 1-cm thick layer containing fine roots. Greater values of absolute root abundances indicate greater presence of fine roots per 1-cm soil layer. Results in (c, d) refer to the normalized root abundance, shown as a percentage of each 1-cm thick soil layer containing fine roots relative to the total roots observed across the profile. Greater values of normalized root abundances indicate greater contribution of roots in 1-cm soil layer relative to the total rooting system. Agricultural systems are displayed in (a, c), and native prairie systems are displayed in (b, d).

(Hinsinger et al., 2009; Lu et al., 2020; Sullivan et al., 2022). Although new pores are formed when roots exert enough pressure to push soil particles aside and create new voids (Hinsinger et al., 2009), as roots grow deeper they are more likely to use existing pores because they offer lower mechanical resistivity and can be hotspots for nutrient availability (Kautz, 2015; Lucas et al., 2019a). There is evidence, however, that roots can also compact the surrounding soil, which appears to be linked to the connectivity of existing macropores in the system (Lucas et al., 2019a). Regardless of the net effect of roots in the soil, their influence on soil structure shapes the pore space in ways significant for the transport of OM, coupling shallower to deep soil layers via water infiltration. The increase in coarse rooting depth abundances with greater effective

precipitation in native prairie systems in Kansas (Fig. 8b) appears to be associated with greater mean aggregate diameters, especially at the surface (Fig. 11b). Preliminary statistical analyses indicate that these features are linked to enhanced total porosity across depth (data not shown), in line with evidence of increased aggregate stability with higher SOM inputs that modify pore distribution in ways that reduce slaking and thus aggregate breakdown (Papadopoulos et al., 2009; Dal Ferro et al., 2012). The drivers of the directionality of linkages between rooting depth distributions, soil aggregate sizes, and soil porosity remain uncertain, but the current work emphasizes the strength of these interactions.

Finally, greater water availability with an increase in E<sub>f</sub>P from west

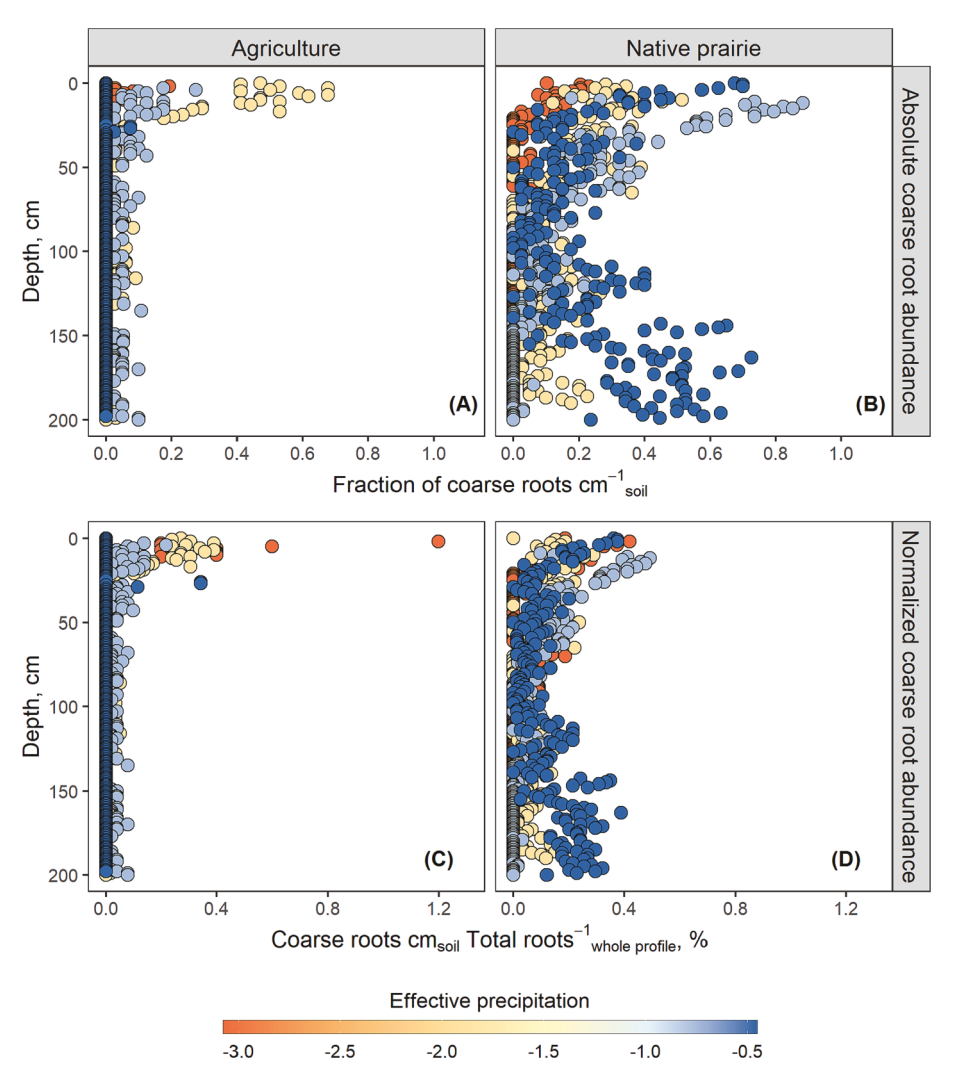


Fig. 8. Coarse rooting depth-distributions across Kansas, USA. Results in (a, b) refer to the absolute root abundance, shown as a fraction of the 1-cm thick layer containing coarse roots. Greater values of absolute root abundances indicate greater presence of coarse roots per 1-cm soil layer. Results in (c, d) refer to the normalized root abundance, shown as a percentage of each 1-cm thick soil layer containing coarse roots relative to the total roots observed across the profile. Greater values of normalized root abundances indicate greater contribution of coarse roots in 1-cm soil layer relative to the total rooting system. Agricultural systems are displayed in (a, c), and native prairie systems are displayed in (b, d).

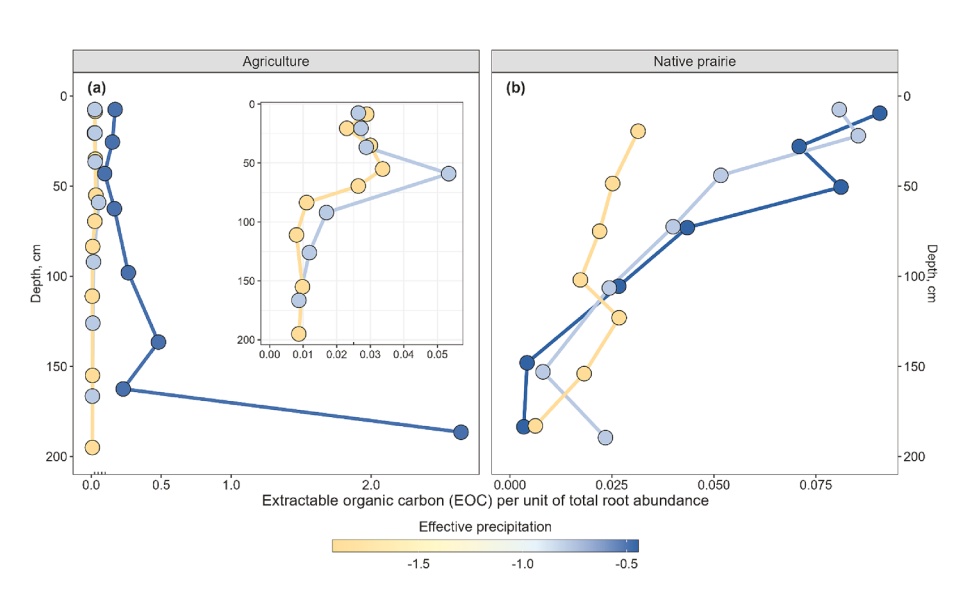
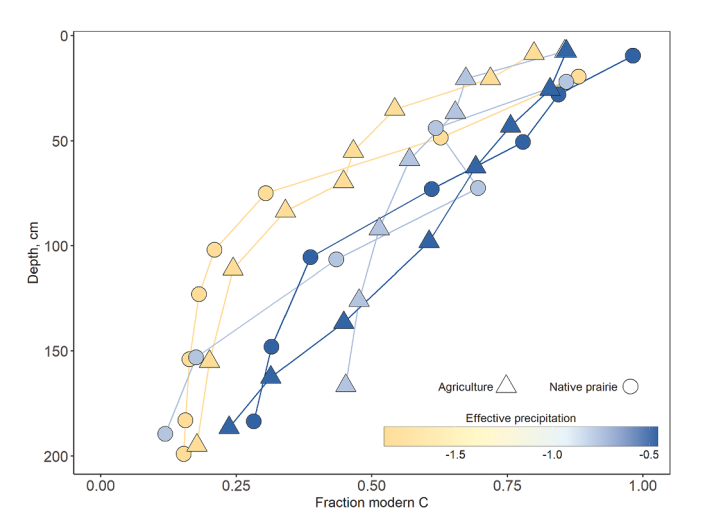


Fig. 9. Extractable organic carbon (EOC) normalized by total root abundances for six profiles across Kansas, USA. Data displayed corresponds to profiles on (a) agricultural and (b) native prairie systems. Inset plot in (a) shows the data within a shorter interval for the EOC per unit of total root abundance. Minor breaks inside the x-axis of (a) represent major breaks in the x-axis of (b).

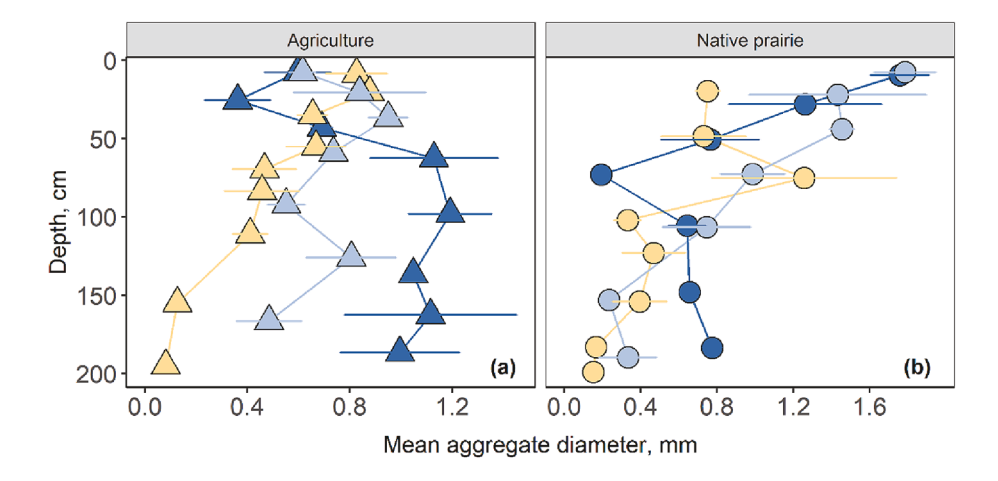


**Fig. 10.** Fraction modern C as derived from  $\Delta^{14}$ C, for six soil profiles sampled across an effective precipitation gradient within the state of Kansas, USA.

to east in the US Midwest may allow greater movement of SOC pools across depths and promote the coupling of surface and subsurface processes (Kaiser and Kalbitz, 2012). Although porosity is an important feature allowing downward flow of C, sufficient moisture is necessary for this transport to happen. When hydrological flows are sufficient, often as a product of subsurface permeability, the water transported down-profile mobilizes resources in a way that promotes the coupling of horizons, as its interactions with roots, microbes, and the soil matrix creates a vertical connectivity between shallow and deeper layers (Kaiser and Kalbitz, 2012; Li et al., 2017; Li et al., 2021; Xiao et al., 2021). Root-driven hydraulic redistribution (Caldwell et al., 1998) may also serve as a source of water that can promote SOC transport throughout a pedon as well (Rumpel and Kögel-Knabner, 2011; Prieto et al., 2012). Such vertical connectivity can be an important influence on a diversity of biogeochemical processes (Kaiser and Kalbitz, 2012; Billings et al., 2018; Podrebarac et al., 2021; Xiao et al., 2021).

#### 4.2. Land-use conversion and SOC depth distributions

The distinct responses of  $\beta$  to  $E_fP$  in agricultural vs. native prairie soils (Fig. 2b, 2c) suggest that agricultural practices in the U.S. Midwest modify the way that SOC inputs respond to variability in the soil moisture that is potentially available to move material within soil



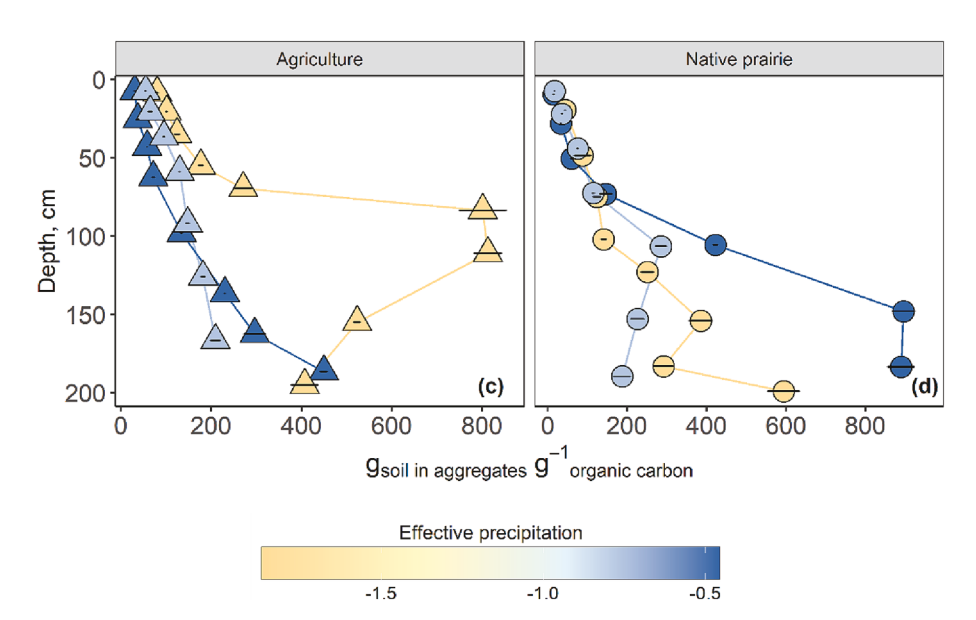


Fig. 11. Water-stable aggregate abundance normalized by SOC for six soil profiles sampled across an effective precipitation gradient with the state of Kansas. (a) and (b) display the mean aggregate diameter for each horizon. (c) and (d) show the proportion of intermediate macroaggregate sizes (between 0.21 and 4.75 mm diameter) per gram of OC for each horizon. Error bars represent the standard deviation of the laboratory replicates.

profiles. This response to E<sub>f</sub>P is a more nuanced way of examining β values than comparing their means across land use; indeed,  $\beta$  for profiles sampled under agriculture in Kansas are not statistically different from those in native prairie (p = 0.573), a result likely reflecting the high variability in estimating the rate of SOC decrease with depth and the relatively low number of pedons sampled (Fig. 6b). However,  $\beta$  responses to E<sub>f</sub>P suggest that shifts in SOC with depth in native prairie soils where moisture availability is greater are less abrupt than in agricultural soils. The shallowing of the rooting system as native prairie is converted to cultivated lands (Jackson et al., 1996; DuPont et al., 2014) and the concurrent loss of surficial SOC (Tang et al., 2019) may limit the degree to which C is distributed throughout agricultural profiles. It is well documented that agricultural practices have led to significant losses of C (Guo and Gifford, 2002; Deng et al., 2016; Tang et al., 2019), an observation that has instigated many other studies looking into the effects of different land managements on the addition, distribution, and decomposition of C (Six et al., 1999; Post and Kwon, 2000; Luo et al., 2010; Deng et al., 2016). Conventional agriculture is responsible for larger rates of erosion than those of soil production (Montgomery, 2007), and the disruption of surficial soils not only redistributes C across the landscape but also leads to soil structural changes that can promote SOC mineralization to CO<sub>2</sub> (Lal, 2003; Quinton et al., 2010; Doetterl et al., 2016). Changes in SOC at surface will thus affect the availability of C to be transported to deep soils, with consequences for C stabilization and its overall depth distribution. The correspondence of  $\beta$  values estimated by SOC concentrations with those derived from SOC stocks (Fig. 4a) suggests that our inferences about the vertical distribution of SOC are robust regardless of which measure is used, and generates similar estimates of the variation in β across the EfP gradient under both land uses calculated from either measurement.

Exponential fits of SOC depth distributions derived from PEDS and the Kansas profiles permitted calculation of  $z_{SOC}$ , the depth at which SOC concentration becomes invariant. This value is considered a threshold for the transition from the dominance of biotic processes in a soil profile to mineralogical processes as the main drivers of C retention (Lawrence et al., 2015; Sulman et al., 2020; White et al., 2012). In a study investigating the parameters of SOC depth distribution across the continental US using C concentrations and C stocks, Sulman et al. (2020) explored variation in  $z_{SOC}$  and found that its deepest values were present in the Central Plains, and deeper for profiles with an Ap horizon. We observed the same trend of deeper z<sub>SOC</sub> estimates under agricultural compared to native prairie sites using PEDS profiles across the US Midwest (Fig. 5), though our results are generally deeper than those observed for Mollisols in Sulman et al. (2020). Moreover, profiles indicating z<sub>SOC</sub> values of 500 cm likely indicate that z<sub>SOC</sub> is probably deeper than the depth interval we used in our predictions (see Section 2.5). Greater z<sub>SOC</sub> depth estimates in the current study relative to those reported in Sulman et al. (2020) may arise from differences in approaches for estimating z<sub>soc</sub>, as we did not use a piecewise function but instead predicted SOC vertical distributions in 1-cm increments down to a predetermined depth. However, deeper thresholds between biotic and "quasi-biotic" processes in cultivated lands implied by data in both studies suggest greater coupling of shallow and deep biogeochemical cycles promoted by agriculture, instead of a perhaps more intuitive decoupling above and below the plow line. Specifically, z<sub>SOC</sub> estimates from PEDS profiles suggest that C-related biogeochemical cycling declines more abruptly with depth in cultivated lands, rather than in agricultural plots where the plow line might be predicted to serve as a physical threshold within C distribution patterns. Estimates of z<sub>SOC</sub> across Kansas further support a greater vertical coupling of biogeochemical cycles under agricultural systems and highlight the significant effect of  $E_fP$  on  $z_{SOC}$ , especially under native prairie soils where the fit of the model was better (Fig. 6c). Moreover, the increase in z<sub>SOC</sub> with greater water availability across Kansas is congruent with an observed decrease in carbonate content which, in turn, suggests that abiotic processes at z<sub>SOC</sub> may decline in relative dominance where moisture availability increases (Gunal and

Ransom, 2006; Fernández-Ugalde et al., 2011). Our findings are in line with the interpretation that  $z_{SOC}$  reflects the depth at which SOC has been relatively insulated from surficial processes and that land conversion may promote the decomposition of deep C with the transport of OC and root exudates throughout soils (Hicks Pries et al., 2017; Sulman et al., 2020).

# 4.3. Exploring the mechanisms governing SOC depth distribution patterns at the pedon scale

To further investigate the mechanisms driving variation in SOC depth distributions across the US Midwest, we analyzed data obtained from soil pits across Kansas for a more complete physical, chemical, and biological characterization of profiles from across the EfP gradient and from native prairie and agricultural lands. Perhaps most notably, we observed clear differences in rooting abundances between the two land uses along the climatic gradient (Fig. 7a, 7b), with the most evident differences in coarse root abundances (Fig. 8a, 8b). Reductions in rooting inputs deep in soil profiles are expected between perennial and annual systems (Canadell et al., 1996; Jackson et al., 1996; DuPont et al., 2014; Billings et al., 2018). Where roots are more abundant, SOC stocks tend to be greater because of greater inputs of solid C material, the greater mean residence time of root C than aboveground C (Rasse et al., 2005; Sokol et al., 2019), and the release of C-rich root exudates in the rhizosphere. Such observations are consistent with our finding of greater EOC concentrations in native prairie soils compared to agricultural soils (Fig. S3), even though normalized root investments, especially those of fine roots, appear similar across the E<sub>f</sub>P gradient (Fig. 7d). The EOC data thus hint at greater availability of SOC easily transformed into solute form with increased root abundance (Fig. S3).

Two lines of evidence suggest that differences in rooting abundances imposed by native prairie conversion to agriculture has prompted soil structural changes that have consequences for transport of SOC, including EOC, and its protection. First, differences in root abundances may dictate the rate at which C such as the EOC pool can flow downward by changing soil porosity (Kaiser and Kalbitz, 2012; Lucas et al., 2019b; Lu et al., 2020). This may have occurred in the current study particularly given differences in coarse roots across land uses (Fig. 8a, 8b), via increased perforation when roots elongate or by leaving open pores after the decay of roots left behind upon land conversion (Fig. 8a; Lu et al., 2020). This idea is supported by generally greater values of EOC per unit total root abundances in agricultural plots across Kansas in horizons between ~40 to ~75 cm at two drier sites, and at the deepest depth sampled at the wettest site (Fig. 9). This feature indicates that some combination of enhanced root production of EOC is occurring at depth in agricultural soils, or that more EOC is infiltrating to depth from shallower horizons in agricultural soils. We cannot know which of these features dominates in these soils, but radiocarbon data also provide a line of evidence suggesting that altered soil structure has modified the extent of soluble OC transport down-profile in these agricultural plots.

Radiocarbon data suggest greater transport of fresh photosynthate from surface horizons deeper into the subsoil in agricultural soils, and greater preservation of SOC in native prairie soils in relatively deeper horizons (Fig. 10). Spatially replicated soil radiocarbon data are difficult to obtain (Schrumpf et al., 2013), but our data are consistent with the idea that land conversion of unplowed systems to croplands may favor the formation of preferential paths through which water can flow, perhaps as decaying coarse roots in converted systems leave behind empty voids (Lu et al., 2020). Flow path formation may be further strengthened in soils with meaningful shrink-swell capacity (Tuller and Or, 2003), which is the case where there are high concentrations of montmorillonite (Schulze, 2005) and relatively high coefficient of linear extensibility (COLE) values (Fig. S4). We note that radiocarbon signatures in relatively deep horizons indicate the greatest FM in agricultural soils where water availability is highest (Fig. 10), corresponding to depths at or below which COLE is greatest (Fig. S4). This observation in

tandem with EOC data per unit total root abundances (Fig. 9) hints that agricultural soils may experience structural changes at multiple depths upon conversion, promoting greater down profile transport of relatively fresh photosynthate.

Radiocarbon data are also consistent with the idea that in deeper horizons, native prairie soils exhibit better ability to retain relatively old SOC (Fig. 10). This may be the case, given that differences in radiocarbon signatures between agricultural and native prairie soils were greater with greater E<sub>f</sub>P, and that intermediate-sized macroaggregates per unit of SOC were greater in native prairie soils at depth with relatively high E<sub>f</sub>P (Fig. 11d). There, SOC seems to promote the formation or preservation of relatively large water-stable aggregates, which appear effective at preserving SOC (Six et al., 2000; Six and Paustian, 2014). In contrast to intermediate-sized macroaggregates per unit SOC, the MAD of water-stable aggregates in agricultural soils increased with depth where E<sub>f</sub>P was high (Fig. 11a). This indicates that agricultural practices at the surface can affect aggregate formation far more deeply than the plow line, particularly where E<sub>f</sub>P is sufficient to promote the propagation of surficial processes to the subsurface. Although we could not conduct statistical analyses at the pedon scale for the soil aggregate data, our work suggests that agriculture may promote formation of larger aggregates as deep as 200 cm as E<sub>f</sub>P increases (Fig. 11a). In agricultural plots, deep SOC promotion of aggregation appears to occur to a greater extent in drier systems (Fig. 11c). This is consistent with the idea of more variable soil moisture promoting greater flashiness of surficial SOC flows down-profile, resulting in greater FM signatures in agricultural systems compared to their native prairie counterparts (Fig. 10). Further work exploring this topic should focus on sampling soil profiles specifically for physical characterization under different land uses at depths equal or greater than what was done in our study with sufficient spatial replicates to allow for more robust statistical analyses.

We note that the degree of clay complexation of SOC is likely an additional, important determinant of water-stable aggregation. The concept of complexed organic C (COC) is a useful tool for understanding drivers of soil structure (Dexter et al., 2008; Klopfenstein et al., 2015; Johannes et al., 2017). Estimates of complexed clay (CC) can inform us about soil stability in water, because non-complexed clay (NCC) is often well correlated to the readily-dispersible clay of a system and may also play a role in defining soil structural conditions (Dexter et al., 2008; Schjønning et al., 2012). Estimates of the total fraction of the system that is complexed, including both COC and CC (TCS; Appendix B), suggests that where SOC is more readily accessible to soil microbes (i.e., where SOC is less complexed; Fig. S5), SOC appears to have a greater propensity to form intermediate-sized macroaggregates (Fig. 11c, 11d), apparently driven by older C (Fig. 10). This is in line with the argument that deep C exhibits a longer transit time (Rumpel and Kögel-Knabner, 2011; Sierra et al., 2017) and that the controls of SOM stabilization are physical protection (Six et al., 2004; Fontaine et al., 2007) and perhaps O<sub>2</sub> availability (Keiluweit et al., 2017). Moreover, these older C signatures may also reflect the fewer inputs of fresh photosynthate to the subsurface, which has been found to increase the longevity of the C storage (Fontaine et al., 2007; Fig. 10). In these Kansans soils, the greater carbonate contents where water availability is limiting (Gunal and Ransom, 2006) is probably another important driver of C protection. Higher Ca<sup>2+</sup> concentrations can promote greater microaggregate stability via the formation of pedogenic carbonates that act as a protective coating (Fernández-Ugalde et al., 2011), consistent with the smaller aggregate size observed under drier systems, especially at depths below the plow line (Fig. 11a, 11b).

Our work thus demonstrates that land management indirectly influences the degree to which SOC can promote or maintain soil aggregate structure across depth (Fig. 11c, 11d). We emphasize the importance of understanding the combined effects of land use and climate on the ecosystem features driving SOC depth distribution. These changes may affect soil structure at depths greater than the plow line, echoing the need to dig deeper to understand changes in rates of

pedological processes in the Anthropocene (Richter, 2020). As a result, soil structure may now be altered on timescales relevant for human lifetimes, far shorter than the geological time periods across which these processes are typically assumed to occur, as has been recently suggested (Hirmas et al., 2018; Sullivan et al., 2022). Rapid soil structural changes have important consequences for understanding and predicting the drivers of C cycling and storage under climate change. We present this study as a starting point from which to generate new hypothesis about how changes to interacting ecosystem features in the Anthropocene, such as rooting depth distributions and soil structure, may control hydrological flow paths and biogeochemical fluxes and transformations in significant ways for the functioning of the Earth's critical zone.

#### 5. Conclusions

Our work investigates the degree to which ecosystem features like effective precipitation and land use conversion interact to govern SOC depth distributions across a climatic gradient in the US Midwest. We found that the vertical distribution of SOC under native prairie soils is more coupled across surficial and deeper horizons where water availability increases. Upon grassland conversion to agriculture, that trend falters. In line with our hypothesis, our work suggests that this shift is the result of changes in rooting abundances and, further, that reduced rooting abundance influences soil structure in ways that can promote vertical flows of water and the transport of C down-profile, which contributes to aggregate stability and SOC protection. Our study highlights the importance of investigating ecosystem features that drive C inputs and depth distributions in tandem with the depth to which land conversion propagates and the timescales over which soil structural changes can occur.

# **Declaration of Competing Interest**

The authors declare that they have no known competing financial interests or personal relationships that could have appeared to influence the work reported in this paper.

# Data availability

The Pedogenic and Environmental DataSet (PEDS) is published in Mohammed et al. (2020). The data and codes that support the findings of this study are available on Zenodo at <a href="https://doi.org/10.5281/zenodo.7892492">https://doi.org/10.5281/zenodo.7892492</a>.

### Acknowledgments

We are grateful for the assistance from John Warner and the National Resources Conservation Service (NRCS-USDA) for help excavating soil profiles and providing additional chemical and physical characterization of these pedons across Kansas (a subset of the SOC concentrations, coefficient of linear extensibility (COLE), clay content, bulk density, and soil taxonomy). We also thank Ariel Mollhagen, Michael Mackenzie, Cheyenne Kirkwood, Jonathan Boyd, and Regina Thomas for laboratory assistance, and the MAPS-EPSCoR team for sampling efforts in Kansas. LS and SB were supported by the National Science Foundation under Award No. OIA-1656006 and matching support from the State of Kansas through the Kansas Board of Regents. Support to DH was provided by Hatch funds (No. CA-R-ENS-5195-H, project accession No. 1022418) and USDA National Institute of Food and Agriculture (NIFA) Signals in the Soil grant (2021-67019-34341; 2021-67019-34338), to SB by a USDA NIFA Signals in the Soil grant (2021-67019-34338), and to DH, PS, and SB by the National Science Foundation's grants 2026874, 2034232, and 2034214. Any opinions, findings, and conclusions or recommendations expressed in this material are those of the authors and do not necessarily reflect the views of the National Science Foundation.

#### Appendix A. Supplementary data

Supplementary data to this article can be found online at https://doi.org/10.1016/j.geoderma.2023.116569.

#### References

- Banwart, S., Bernasconi, S.M., Bloem, J., Blum, W., Brandao, M., Brantley, S., Chabaux, F., Duffy, C., Kram, P., Lair, G., Lundin, L., Nikolaidis, N., Novak, M., Panagos, P., Ragnarsdottir, K.V., Reynolds, B., Rousseva, S., de Ruiter, P., van Gaans, P., van Riemsdijk, W., White, T., Zhang, B., 2011. Soil processes and functions in critical zone observatories: hypotheses and experimental design. Vadose Zone J. 10 (3), 974–987.
- Banwart, S.A., Nikolaidis, N.P., Zhu, Y.-G., Peacock, C.L., Sparks, D.L., 2019. Soil functions: connecting earth's critical zone. Annu. Rev. Earth Planet Sci. 47 (1), 333–359. https://doi.org/10.1146/annurev-earth-063016-020544.
- Bartlett, R.J., Ross, D.S., 1988. Colorimetric determination of oxidizable carbon in acid soil solutions. Soil Sci. Soc. Am. J. 52 (4), 1191–1192. https://doi.org/10.2136/ sssaj1988.03615995005200040055x.
- Beillouin, D., Cardinael, R., Berre, D., Boyer, A., Corbeels, M., Fallot, A., Feder, F., Demenois, J., 2022. A global overview of studies about land management, land-use change, and climate change effects on soil organic carbon. Glob Change Biol. 28 (4), 1690–1702. https://doi.org/10.1111/gcb.15998.
- Billings, S.A., Hirmas, D., Sullivan, P.L., Lehmeier, C.A., Bagchi, S., Min, K., Brecheisen, Z., Hauser, E., Stair, R., Flournoy, R., et al. 2018. Loss of deep roots limits biogenic agents of soil development that are only partially restored by decades of forest regeneration. Chadwick O, editor. Elem. Sci. Anthr., 6: 34. doi: 10.1525/elementa.287.
- Bos, M.G., Kselik, R.A.L., Allen, R.A., Molden, D.J., 2009. Effective precipitation. In: Water Requirements for Irrigation and the Environment. 1st ed. Dordrecht: Springer Netherlands. p. 81–101. doi: 10.1007/978-1-4020-8948-0 3.
- Bowering, K.L., Edwards, K.A., Wiersma, Y.F., Billings, S.A., Warren, J., Skinner, A., Ziegler, S.E., 2023. Dissolved organic carbon mobilization across a climate transect of mesic boreal forests is explained by air temperature and snowpack duration. *Ecosystems* 26 (1), 55–71.
- Bradford, M.A., Wieder, W.R., Bonan, G.B., Fierer, N., Raymond, P.A., Crowther, T.W., 2016. Managing uncertainty in soil carbon feedbacks to climate change. Nat. Clim. Change 6 (8), 751–758. https://doi.org/10.1038/nclimate3071.
- Brantley, S.L., Eissenstat, D.M., Marshall, J.A., Godsey, S.E., Balogh-Brunstad, Z., Karwan, D.L., Papuga, S.A., Roering, J., Dawson, T.E., Evaristo, J., Chadwick, O., McDonnell, J.J., Weathers, K.C., 2017. Reviews and syntheses: on the roles trees play in building and plumbing the critical zone. Biogeosciences 14 (22), 5115–5142.
- Bronick, C.J., Lal, R., 2005. Soil structure and management: a review. Geoderma 124 (1–2), 3–22. https://doi.org/10.1016/j.geoderma.2004.03.005.
- Caldwell, M.M., Dawson, T.E., Richards, J.H., 1998. Hydraulic lift: consequences of water efflux from the roots of plants. Oecologia 113 (2), 151–161. https://doi.org/ 10.1007/s004420050363.
- Canadell, J., Jackson, R.B., Ehleringer, J.B., Mooney, H.A., Sala, O.E., Schulze, E.-D., 1996. Maximum rooting depth of vegetation types at the global scale. Oecologia 108 (4), 583–595. https://doi.org/10.1007/BF00329030.
- Cherkinsky, A., Culp, R.A., Dvoracek, D.K., Noakes, J.E., 2010. Status of the AMS facility at the University of Georgia. Nucl. Instrum. Methods Phys. Res. Sect. B Beam Interact. Mater. At. 268 (7–8), 867–870. https://doi.org/10.1016/j. nimb.2009.10.051.
- Cherkinsky, A., Brecheisen, Z., Richter, D., 2018. Carbon and oxygen isotope composition in soil carbon dioxide and free oxygen within deep ultisols at the calhoun CZO, South Carolina, USA. Radiocarbon 60 (5), 1357–1366. https://doi. org/10.1017/RDC.2018.99.
- Conant, R.T., Cerri, C.E.P., Osborne, B.B., Paustian, K., 2017. Grassland management impacts on soil carbon stocks: a new synthesis. Ecol. Appl. 27 (2), 662–668. https://doi.org/10.1002/eap.1473.
- Crowther, T.W., Todd-Brown, K.E.O., Rowe, C.W., Wieder, W.R., Carey, J.C., Machmuller, M.B., Snoek, B.L., Fang, S., Zhou, G., Allison, S.D., Blair, J.M., Bridgham, S.D., Burton, A.J., Carrillo, Y., Reich, P.B., Clark, J.S., Classen, A.T., Dijkstra, F.A., Elberling, B., Emmett, B.A., Estiarte, M., Frey, S.D., Guo, J., Harte, J., Jiang, L., Johnson, B.R., Kröel-Dulay, G., Larsen, K.S., Laudon, H., Lavallee, J.M., Luo, Y., Lupascu, M., Ma, L.N., Marhan, S., Michelsen, A., Mohan, J., Niu, S., Pendall, E., Penuelas, J., Pfeifer-Meister, L., Poll, C., Reinsch, S., Reynolds, L.L., Schmidt, I.K., Sistla, S., Sokol, N.W., Templer, P.H., Treseder, K.K., Welker, J.M., Bradford, M.A., 2016. Quantifying global soil carbon losses in response to warming. Nature 540 (7631), 104–108.
- Dal Ferro, N., Berti, A., Francioso, O., Ferrari, E., Matthews, G.P., Morari, F., 2012. Investigating the effects of wettability and pore size distribution on aggregate stability: the role of soil organic matter and the humic fraction. Eur. J. Soil Sci. 63 (2), 152–164. https://doi.org/10.1111/j.1365-2389.2012.01427.x.
- Davidson, E.A., Janssens, I.A., 2006. Temperature sensitivity of soil carbon decomposition and feedbacks to climate change. Nature 440 (7081), 165–173. https://doi.org/10.1038/nature04514.
- Davidson, E.A., Trumbore, S.E., Amundson, R., 2000. Soil warming and organic carbon content. Nature 408 (6814), 789–790. https://doi.org/10.1038/35048672.
- Deng, L., Zhu, G., Tang, Z., Shangguan, Z., 2016. Global patterns of the effects of land-use changes on soil carbon stocks. Glob Ecol. Conserv. 5, 127–138. https://doi.org/ 10.1016/j.gecco.2015.12.004.

- Dexter, A.R., 1987. Mechanics of root growth. Plant Soil 98 (3), 303–312. https://doi. org/10.1007/BF02378351.
- Dexter, A.R., 1988. Advances in characterization of soil structure. Soil Tillage Res. 11 (3–4), 199–238. https://doi.org/10.1016/0167-1987(88)90002-5.
- Dexter, A.R., Richard, G., Arrouays, D., Czyż, E.A., Jolivet, C., Duval, O., 2008. Complexed organic matter controls soil physical properties. Geoderma 144 (3–4), 620–627. https://doi.org/10.1016/j.geoderma.2008.01.022.
- Dickson, E.L., Rasiah, V., Groenevelt, P.H., 1991. Comparison of four prewetting techniques in wet aggregate stability determination. Can. J. Soil Sci. 71 (1), 67–72. https://doi.org/10.4141/cjss91-006.
- Doetterl, S., Berhe, A.A., Nadeu, E., Wang, Z., Sommer, M., Fiener, P., 2016. Erosion, deposition and soil carbon: A review of process-level controls, experimental tools and models to address C cycling in dynamic landscapes. Earth-Sci. Rev. 154, 102–122. https://doi.org/10.1016/j.earscirev.2015.12.005.
- DuPont, S.T., Beniston, J., Glover, J.D., Hodson, A., Culman, S.W., Lal, R., Ferris, H., 2014. Root traits and soil properties in harvested perennial grassland, annual wheat, and never-tilled annual wheat. Plant Soil 381 (1–2), 405–420. https://doi.org/ 10.1007/s11104-014-2145-2.
- Fan, J., McConkey, B., Wang, H., Janzen, H., 2016. Root distribution by depth for temperate agricultural crops. Field Crops Res. 189, 68–74. https://doi.org/10.1016/ j.fcr.2016.02.013.
- Fatichi, S., Or, D., Walko, R., Vereecken, H., Young, M.H., Ghezzehei, T.A., Hengl, T., Kollet, S., Agam, N., Avissar, R., 2020. Soil structure is an important omission in Earth System Models. Nat. Commun. 11 (1), 522. https://doi.org/10.1038/s41467-020-14411-z.
- Fernández-Ugalde, O., Virto, I., Barré, P., Gartzia-Bengoetxea, N., Enrique, A., Imaz, M. J., Bescansa, P., 2011. Effect of carbonates on the hierarchical model of aggregation in calcareous semi-arid Mediterranean soils. Geoderma 164 (3–4), 203–214. https://doi.org/10.1016/j.geoderma.2011.06.008.
- Fick, S.E., Hijmans, R.J., 2017. WorldClim 2: new 1-km spatial resolution climate surfaces for global land areas. Int. J. Climatol. 37 (12), 4302–4315. https://doi.org/ 10.1002/joc.5086.
- Fontaine, S., Barot, S., Barré, P., Bdioui, N., Mary, B., Rumpel, C., 2007. Stability of organic carbon in deep soil layers controlled by fresh carbon supply. Nature 450 (7167), 277–280. https://doi.org/10.1038/nature06275.
- Franzluebbers, A.J., 2021. Soil organic carbon sequestration calculated from depth distribution. Soil Sci. Soc. Am. J. 85 (1), 158–171. https://doi.org/10.1002/sai2.20176.
- Ghezzehei, T.A., 2011. Soil structure. In: Huang, P.M., Li, Y., Sumner, M.E. (Eds.), Handbook of Soil Sciences: Properties and Processes, 2nd ed. CRC Press, Boca Raton, FL, pp. 1–17.
- Gould, I.J., Quinton, J.N., Weigelt, A., De Deyn, G.B., Bardgett, R.D., Seabloom, E., 2016.
  Plant diversity and root traits benefit physical properties key to soil function in grasslands. Ecol. Lett. 19 (9), 1140–1149.
- Gunal, H., Ransom, M.D., 2006. Clay illuviation and calcium carbonate accumulation along a precipitation gradient in Kansas. Catena 68 (1), 59–69. https://doi.org/ 10.1016/j.catena.2006.04.027.
- Guo, L.B., Gifford, R.M., 2002. Soil carbon stocks and land use change: a meta analysis. Glob Change Biol. 8 (4), 345–360. https://doi.org/10.1046/j.1354-1013.2002.00486.x.
- Hauser, E., Richter, D.D., Markewitz, D., Brecheisen, Z., Billings, S.A., 2020. Persistent anthropogenic legacies structure depth dependence of regenerating rooting systems and their functions. Biogeochem 147 (3), 259–275. https://doi.org/10.1007/ s10533-020-00641-2.
- Hauser, E., Sullivan, P.L., Flores, A.N., Hirmas, D., Billings, S.A., 2022. Global-scale shifts in rooting depths due to Anthropocene land cover changes pose unexamined consequences for Critical Zone Functioning. Earth's Future 10 (11), 1–14. https:// doi.org/10.1029/2022FF002897.
- Haynes, R.J., Naidu, R., 1998. Influence of lime, fertilizer and manure applications on soil organic matter content and soil physical conditions: a review. Nutr. Cycl. Agroecosystems 51 (2), 123–137. https://doi.org/10.1023/A:1009738307837.
- Heisler-White, J.L., Blair, J.M., Kelly, E.F., Harmoney, K., Knapp, A.K., 2009. Contingent productivity responses to more extreme rainfall regimes across a grassland biome. Glob. Change Biol. 15 (12), 2894–2904. https://doi.org/10.1111/j.1365-2486.2009.01961.x.
- Helliwell, J.R., Sturrock, C.J., Mairhofer, S., Craigon, J., Ashton, R.W., Miller, A.J., Whalley, W.R., Mooney, S.J., 2017. The emergent rhizosphere: imaging the development of the porous architecture at the root-soil interface. Sci. Rep. 7 (1), 14875. https://doi.org/10.1038/s41598-017-14904-w.
- Herbert, B.E., Bertsch, P.M., 2006. Characterization of dissolved and colloidal organic matter in soil solution: a review. In: McFee, W.W., Kelly, J.M. (Eds.), Carbon Forms and Functions in Forest Soils. Soil Science Society of America, Madison, WI, USA, pp. 63–88. https://doi.org/10.2136/1995.carbonforms.c5.
- Hicks Pries, C.E., Castanha, C., Porras, R.C., Torn, M.S., 2017. The whole-soil carbon flux in response to warming. Science 355 (6332), 1420–1423. https://doi.org/10.1126/ science.aal1319.
- Hinsinger, P., Bengough, A.G., Vetterlein, D., Young, I.M., 2009. Rhizosphere: biophysics, biogeochemistry and ecological relevance. Plant Soil 321 (1–2), 117–152. https://doi.org/10.1007/s11104-008-9885-9.
- Hirmas, D.R., Giménez, D., Nemes, A., Kerry, R., Brunsell, N.A., Wilson, C.J., 2018. Climate-induced changes in continental-scale soil macroporosity may intensify water cycle. Nature 561 (7721), 100–103. https://doi.org/10.1038/s41586-018-0463-x.
- Houghton, R.A., 1995. Land-use change and the carbon cycle. Glob. Change Biol. 1 (4), 275–287. https://doi.org/10.1111/j.1365-2486.1995.tb00026.x.

- Jackson, R.B., Canadell, J., Ehleringer, J.R., Mooney, H.A., Sala, O.E., Schulze, E.D., 1996. A global analysis of root distributions for terrestrial biomes. Oecologia 108 (3), 389-411. https://doi.org/10.1007/BF00333714.
- Jackson, R.B., Schenk, H.J., Jobbágy, E.G., Canadell, J., Colello, G.D., Dickinson, R.E., Field, C.B., Friedlingstein, P., Heimann, M., Hibbard, K., et al., 2000. Belowground consequences of vegetation change and their treatment in models. Ecol. Appl. 10 (2), 470-483. https://doi.org/10.1890/1051-0761(2000)010[0470:BCOVCA]
- Jackson, R.B., Lajtha, K., Crow, S.E., Hugelius, G., Kramer, M.G., Piñeiro, G., 2017. The ecology of soil carbon: pools, vulnerabilities, and biotic and abiotic controls. Annu. Rev. Ecol. Evol. Syst. 48 (1), 419-445. https://doi.org/10.1146/annurev-ecolsys-
- Jangid, K., Williams, M.A., Franzluebbers, A.J., Blair, J.M., Coleman, D.C., Whitman, W. B., 2010. Development of soil microbial communities during tallgrass prairie restoration. Soil Biol. Biochem. 42 (2), 302-312. https://doi.org/10.1016/j.
- Jobbágy, E.G., Jackson, R.B., 2000. The vertical distribution of soil organic carbon and its relation to climate and vegetation. Ecol. Appl. 10(2): 423-436. doi: doi.org/ 10.1890/1051-0761(2000)010[0423:TVDOSO]2.0.CO;2.
- Johannes, A., Matter, A., Schulin, R., Weisskopf, P., Baveye, P.C., Boivin, P., 2017. Optimal organic carbon values for soil structure quality of arable soils. does clay content matter? Geoderma 302, 14-21. https://doi.org/10.1016/j.
- Kaiser, K., Kalbitz, K., 2012. Cycling downwards dissolved organic matter in soils. Soil Biol. Biochem. 52, 29-32. https://doi.org/10.1016/j.soilbio.2012.04.002.
- Kalbitz, K., Kaiser, K., 2008. Contribution of dissolved organic matter to carbon storage in forest mineral soils. J. Plant Nutr. Soil Sci. 171 (1), 52-60. https://doi.org/ 10.1002/ipln.200700043.
- Kautz, T., 2015. Research on subsoil biopores and their functions in organically managed soils: A review. Renew. Agric. Food Syst. 30 (4), 318-327. https://doi.org/10.1017/ S1742170513000549.
- Keiluweit, M., Wanzek, T., Kleber, M., Nico, P., Fendorf, S., 2017. Anaerobic microsites have an unaccounted role in soil carbon stabilization. Nat. Commun. 8 (1), 1771. https://doi.org/10.1038/s41467-017-01406-6.
- Kettle, W.D., 2016. The University of Kansas field station: a platform for studying ecological and hydrological aspects of climate change. Trans. Kans. Acad Sci. 119 (1), 12-20, https://doi.org/10.1660/062.119.0104.
- Kleidon, A., Heimann, M., 1998. Optimised rooting depth and its impacts on the simulated climate of an atmospheric general circulation model. Geophys. Res. Lett. 25 (3), 345-348. https://doi.org/10.1029/98GL00034
- Klopfenstein, S.T., Hirmas, D.R., Johnson, W.C., 2015. Relationships between soil organic carbon and precipitation along a climosequence in loess-derived soils of the Central Great Plains, USA. Catena 133, 25–34. https://doi.org/10.1016/j catena, 2015, 04, 015.
- Koenker, R., 2021. Quantreg: Quantile Regression. Available at https://CRAN.R-project.
- org/package=quantreg.
  Koop, A.N., Hirmas, D.R., Sullivan, P.L., Mohammed, A.K., 2020. A generalizable index of soil development. Geoderma 360, 113898. https://doi.org/10.1016/j. oderma 2019 113898.
- Lal, R., 2003. Soil erosion and the global carbon budget. Environ. Int. 29 (4), 437–450. https://doi.org/10.1016/S0160-4120(02)00192-5
- Lal, R., 2004. Soil carbon sequestration to mitigate climate change. Geoderma 123 (1-2), 1-22. https://doi.org/10.1016/j.geoderma.2004.01.032.
- Lawrence, C.R., Harden, J.W., Xu, X., Schulz, M.S., Trumbore, S.E., 2015. Long-term controls on soil organic carbon with depth and time: a case study from the Cowlitz River Chronosequence, WA USA. Geoderma 247-248, 73-87. https://doi.org/ 10.1016/j.geoderma, 2015.02.005.
- Le Bissonnais, Y., Prieto, I., Roumet, C., Nespoulous, J., Metayer, J., Huon, S., Villatoro, M., Stokes, A., 2018. Soil aggregate stability in Mediterranean and tropical agro-ecosystems: effect of plant roots and soil characteristics. Plant Soil 424 (1-2), 303-317. https://doi.org/10.1007/s11104-017-3423-6
- Li, L., Bao, C., Sullivan, P.L., Brantley, S., Shi, Y., Duffy, C., 2017. Understanding watershed hydrogeochemistry: 2. Synchronized hydrological and geochemical processes drive stream chemostatic behavior: concentration-discharge relationship. Water Resour. Res. 53 (3), 2346-2367. https://doi.org/10.1002/2016WR018
- Li, L.i., Sullivan, P.L., Benettin, P., Cirpka, O.A., Bishop, K., Brantley, S.L., Knapp, J.L.A., Meerveld, I., Rinaldo, A., Seibert, J., Wen, H., Kirchner, J.W., 2021. Toward catchment hydro-biogeochemical theories. WIREs Water 8 (1). https://doi.org/
- Lorenz, K., Lal, R., 2005. The depth distribution of soil organic carbon in relation to land use and the potential of carbon sequestration in subsoil horizons. Adv. Agron. 88, 35-66. https://doi.org/10.1016/S0065-2113(05)88002-2.
- Loveland, P., Webb, J., 2003. Is there a critical level of organic matter in the agricultural soils of temperate regions: a review. Soil Tillage Res. 70 (1), 1-18. https://doi.org/ 10.1016/S0167-1987(02)00139-
- Lu, J., Zhang, Q., Werner, A.D., Li, Y., Jiang, S., Tan, Z., 2020. Root-induced changes of soil hydraulic properties - A review. J. Hydrol. 589, 125203 https://doi.org 10.1016/j.jhydrol.2020.125203
- Lucas, M., Schlüter, S., Vogel, H.-J., Vetterlein, D., 2019a. Roots compact the surrounding soil depending on the structures they encounter. Sci. Rep. 9 (1), 16236. //doi.org/10.1038/s41598-019-52665-
- Lucas, M., Schlüter, S., Vogel, H.-J., Vetterlein, D., 2019b. Soil structure formation along an agricultural chronosequence. Geoderma 350, 61-72. https://doi.org/10.1016/j. geoderma.2019.04.041.
- Luo, Z., Wang, E., Sun, O.J., 2010. Can no-tillage stimulate carbon sequestration in agricultural soils? A meta-analysis of paired experiments. Agric. Ecosyst. Environ. 139 (1-2), 224-231. https://doi.org/10.1016/j.agee.2010.08.006.

Marek, G., Gowda, P., Marek, T., Auvermann, B., Evett, S., Colaizzi, P., Brauer, D., 2016. Estimating preseason irrigation losses by characterizing evaporation of effective precipitation under bare soil conditions using large weighing lysimeters. Agric. Water Manag. 169, 115-128. https://doi.org/10.1016/j.agwat.2016.02.024.

- Marín-Spiotta, E., Gruley, K.E., Crawford, J., Atkinson, E.E., Miesel, J.R., Greene, S., Cardona-Correa, C., Spencer, R.G.M., 2014. Paradigm shifts in soil organic matter research affect interpretations of aquatic carbon cycling: transcending disciplinary and ecosystem boundaries. Biogeochemistry 117 (2-3), 279-297. https://doi.org.
- Martinez, P., Buurman, P., do Nascimento, D.L., Almquist, V., Vidal-Torrado, P., 2021. Substantial changes in podzol morphology after tree-roots modify soil porosity and hydrology in a tropical coastal rainforest. Plant Soil 463 (1-2), 77-95.
- Meurer, K.H.E., Chenu, C., Coucheney, E., Herrmann, A.M., Keller, T., Kätterer, T., Nimblad Svensson, D., Jarvis, N., 2020. Modelling dynamic interactions between soil structure and the storage and turnover of soil organic matter. Biogeosciences 17 (20), 5025-5042. https://doi.org/10.5194/bg-17-5025-2020.
- Minasny, B., McBratney, A.B., 2018. Limited effect of organic matter on soil available water capacity. Eur. J. Soil Sci. 69 (1), 39-47. https://doi.org/10.1111/ejss.12475.
- Minasny, B., AlexB, McBratney, Mendonça-Santos, M.L., Odeh, I.O.A., Guyon, B., 2006. Prediction and digital mapping of soil carbon storage in the Lower Namoi Valley. Soil Res 44 (3), 233. https://doi.org/10.1071/SR05136.
- Mishra, U., Lal, R., Slater, B., Calhoun, F., Liu, D., Van Meirvenne, M., 2009. Predicting soil organic carbon stock using profile depth distribution functions and ordinary kriging. Soil Sci. Soc. Am. J. 73 (2), 614-621. https://doi.org/10.2136/
- Mohammed, A.K., Hirmas, D.R., Nemes, A., Giménez, D., 2020. Exogenous and endogenous controls on the development of soil structure. Geoderma 357, 113945. https://doi.org/10.1016/j.geoderma.2019.113945
- Montgomery, D.R., 2007. Soil erosion and agricultural sustainability. Proc. Natl. Acad. Sci. 104 (33), 13268-13272. https://doi.org/10.1073/pnas.0611508104.
- Motew, M.M., Kucharik, C.J., 2013. Climate-induced changes in biome distribution, NPP, and hydrology in the Upper Midwest U.S.: A case study for potential vegetation: CLIMATE IMPACTS IN THE UPPER MIDWEST U.S. J. Geophys. Res. Biogeosciences 118 (1), 248-264. https://doi.org/10.1002/jgrg.20025.
- Nelder, J.A., Mead, R., 1965. A simplex method for function minimization. Comput. J. 7 (4), 308–313. https://doi.org/10.1093/comjnl/7.4.308.
- Nimmo, J.R., Perkins, K.S., 2002. Aggregate stability and size distribution. In: Methods of Soil Analysis, Part 4: Physical Methods. Soil Science Society of America, Madison, Wisconsin, pp. 317-328.
- Papadopoulos, A., Bird, N.R.A., Whitmore, A.P., Mooney, S.J., 2009. Investigating the effects of organic and conventional management on soil aggregate stability using Xray computed tomography. Eur. J. Soil Sci. 60 (3), 360-368. https://doi.org/ 10.1111/j.1365-2389.2009.01126.x.
- Pausch, J., Kuzyakov, Y., 2018. Carbon input by roots into the soil: Quantification of rhizodeposition from root to ecosystem scale, Glob, Change Biol, 24 (1), 1–12, https://doi.org/10.1111/gcb.13850.
- Podrebarac, F.A., Billings, S.A., Edwards, K.A., Laganière, J., Norwood, M.J., Ziegler, S. E., 2021. Soil profile connectivity can impact microbial substrate use, affecting how soil CO<sub>2</sub> effluxes are controlled by temperature. Biogeosciences 18 (16), 4755-4772. https://doi.org/10.5194/bg-18-4755-2021.
- Post, W.M., Kwon, K.C., 2000. Soil carbon sequestration and land-use change: processes and potential. Glob. Change Biol. 6 (3), 317-327. https://doi.org/10.1046/j.1365 2486 2000 00308 x
- Prieto, I., Armas, C., Pugnaire, F.I., 2012. Water release through plant roots: new insights into its consequences at the plant and ecosystem level. New Phytol. 193 (4), 830-841. https://doi.org/10.1111/j.1469-8137.2011.04039.x
- PRISM. 2021. PRISM Climate Group, Oregon State University. Available at https://prism. oregonstate.edu. Accessed 2022 May 25.
- Quinton, J.N., Govers, G., Van Oost, K., Bardgett, R.D., 2010. The impact of agricultural soil erosion on biogeochemical cycling. Nat. Geosci. 3 (5), 311-314. https://doi.org. 10.1038/ngeo838.
- R Core Team, 2022. R: A Language and Environment for Statistical Computing. R Foundation for Statistical Computing, Vienna, Austria. Available at https://www.Rproject.org/.
- Rahmani, V., Harrington, J., 2019. Assessment of climate change for extreme precipitation indices: A case study from the central United States. Int. J. Climatol. 39 (2), 1013-1025. https://doi.org/10.1002/joc.5858.
- Ramnarine, R., Voroney, R.P., Wagner-Riddle, C., Dunfield, K.E., 2011. Carbonate removal by acid fumigation for measuring the  $\delta^{\,13}$  C of soil organic carbon. Can. J. Soil Sci. 91 (2), 247-250. https://doi.org 10.4141/cjss10066
- Rasse, D.P., Rumpel, C., Dignac, M.-F., 2005. Is soil carbon mostly root carbon? Mechanisms for a specific stabilisation. Plant Soil 269 (1-2), 341-356. https://doi. org/10.1007/s11104-004-0907-y
- Rawls, W.J., Pachepsky, Y.A., Ritchie, J.C., Sobecki, T.M., Bloodworth, H., 2003. Effect of soil organic carbon on soil water retention. Geoderma 116 (1-2), 61-76. https:// doi.org/10.1016/S0016-7061(03)00094-6
- Richter, D.D., 2020. Game changer in soil science. The Anthropocene in soil science and pedology. J. Plant Nutr. Soil Sci. 183 (1), 5-11. https://doi.org/10.1002/ jpln.201900320.
- Ruehlmann, J., Körschens, M., 2009. Calculating the effect of soil organic matter concentration on soil bulk density. Soil Sci. Soc. Am. J. 73 (3), 876-885. https://doi. org/10.2136/sssaj2007.0149.
- Rumpel, C., Kögel-Knabner, I., 2011. Deep soil organic matter—a key but poorly understood component of terrestrial C cycle. Plant Soil 338 (1-2), 143-158. https:// doi.org/10.1007/s11104-010-0391-5.

- Saxton, K.E., Rawls, W.J., 2006. Soil water characteristic estimates by texture and organic matter for hydrologic solutions. Soil Sci. Soc. Am. J. 70 (5), 1569–1578. https://doi.org/10.2136/sssaj2005.0117.
- Saxton, K.E., Rawls, W.J., Romberger, J.S., Papendick, R.I., 1986. Estimating generalized soil-water characteristics from texture. Soil Sci. Soc. Am. J. 50 (4), 1031–1036. https://doi.org/10.2136/sssaj1986.03615995005000040039x.
- Schenk, H.J., Jackson, R.B., 2002. Rooting depths, lateral root spreads and below-ground/above-ground allometries of plants in water-limited ecosystems. J. Ecol. 90 (3), 480–494. https://doi.org/10.1046/j.1365-2745.2002.00682.x.
- Schjønning, P., de Jonge, L.W., Munkholm, L.J., Moldrup, P., Christensen, B.T., Olesen, J. E., 2012. Clay dispersibility and soil friability-testing the soil clay-to-carbon saturation concept. Vadose Zone J. 11 (1) https://doi.org/10.2136/vzj2011.0067.
- Schrumpf, M., Kaiser, K., Guggenberger, G., Persson, T., Kögel-Knabner, I., Schulze, E.-D., 2013. Storage and stability of organic carbon in soils as related to depth, occlusion within aggregates, and attachment to minerals. Biogeosciences 10 (3), 1675–1691. https://doi.org/10.5194/bg-10-1675-2013.
- Schulze, D.G., 2005. Clay minerals. In: Encyclopedia of Soils in the Environment. Elsevier, pp. 246–254.
- Schwendenmann, L., Pendall, E., 2006. Effects of forest conversion into grassland on soil aggregate structure and carbon storage in Panama: evidence from soil carbon fractionation and stable isotopes. Plant Soil 288 (1–2), 217–232. https://doi.org/ 10.1007/s11104-006-9109-0.
- Sierra, C.A., Müller, M., Metzler, H., Manzoni, S., Trumbore, S.E., 2017. The muddle of ages, turnover, transit, and residence times in the carbon cycle. Glob Change Biol. 23 (5), 1763–1773. https://doi.org/10.1111/gcb.13556.
- Six, J., Elliott, E.T., Paustian, K., 1999. Aggregate and soil organic matter dynamics under conventional and no-tillage systems. Soil Sci. Soc. Am. J. 63 (5), 1350–1358. https://doi.org/10.2136/sssaj1999.6351350x.
- Six, J., Elliott, E.T., Paustian, K., 2000. Soil macroaggregate turnover and microaggregate formation: a mechanism for C sequestration under no-tillage agriculture. Soil Biol. Biochem. 32 (14), 2099–2103. https://doi.org/10.1016/S0038-0717(00)00179-6.
- Six, J., Bossuyt, H., Degryze, S., Denef, K., 2004. A history of research on the link between (micro)aggregates, soil biota, and soil organic matter dynamics. Soil Tillage Res. 79 (1), 7–31. https://doi.org/10.1016/j.still.2004.03.008.
- Six, J., Paustian, K., 2014. Aggregate-associated soil organic matter as an ecosystem property and a measurement tool. Soil Biol. Biochem. 68, A4–A9. https://doi.org/ 10.1016/j.soilbio.2013.06.014.
- Sokol, N.W., Bradford, M.A., 2019. Microbial formation of stable soil carbon is more efficient from belowground than aboveground input. Nat. Geosci. 12 (1), 46–53. https://doi.org/10.1038/s41561-018-0258-6.
- Sokol, N.W., SaraE, K., Karlsen-Ayala, E., Bradford, M.A., 2019. Evidence for the primacy of living root inputs, not root or shoot litter, in forming soil organic carbon. New Phytol. 221 (1), 233–246. https://doi.org/10.1111/nph.15361.
- Sullivan, P.L., Billings, S.A., Hirmas, D., Li, L., Zhang, X., Ziegler, S., Murenbeeld, K., Ajami, H., Guthrie, A., Singha, K., Giménez, D., Duro, A., Moreno, V., Flores, A.,

- Cueva, A., Koop, Aronson, E.L., Barnard, H.R., Banwart, S.A., Keen, R.M., Nemes, A., Nikolaidis, N.P., Nippert, J.B., Richter, D., Robinson, D.A., Sadayappan, K., de Souza, L.F.T., Unruh, M., Wen, H., 2022. Embracing the dynamic nature of soil structure: A paradigm illuminating the role of life in critical zones of the Anthropocene. Earth-Sci. Rev. 225, 103873.
- Sulman, B.N., Harden, J., He, Y., Treat, C., Koven, C., Mishra, U., O'Donnell, J.A., Nave, L.E., 2020. Land use and land cover affect the depth distribution of soil carbon: insights from a large database of soil profiles. Front. Environ. Sci. 8, 146. https://doi.org/10.3389/fenvs.2020.00146.
- Sun, T., Wang, Y., Hui, D., Jing, X., Feng, W., 2020. Soil properties rather than climate and ecosystem type control the vertical variations of soil organic carbon, microbial carbon, and microbial quotient. Soil Biol. Biochem. 148, 107905 https://doi.org/ 10.1016/j.soilbio.2020.107905
- Tang, S., Guo, J., Li, S., Li, J., Xie, S., Zhai, X., Wang, C., Zhang, Y., Wang, K., 2019. Synthesis of soil carbon losses in response to conversion of grassland to agriculture land. Soil Tillage Res. 185, 29–35. https://doi.org/10.1016/j.still.2018.08.011.
- Tisdall, J.M., Oades, J.M., 1982. Organic matter and water-stable aggregates in soils. J. Soil Sci. 33 (2), 141–163. https://doi.org/10.1111/j.1365-2389.1982.tb01755.x.
- Trabucco, A., Zomer, R.J., 2018. Global Aridity Index and Potential Evapo-Transpiration (ETO) Climate Database v2. CGIAR Consortium for Spatial Information (CGIAR-CSI). Published online, available from the CGIAR-CSI GeoPortal at https://cgiarcsi.community.
- Trumbore, S., 2009. Radiocarbon and soil carbon dynamics. Annu. Rev. Earth Planet Sci. 37 (1), 47–66. https://doi.org/10.1146/annurev.earth.36.031207.124300.
- Tuller, M., Or, D., 2003. Hydraulic functions for swelling soils: pore scale considerations. J Hydrol 272 (1–4), 50–71. https://doi.org/10.1016/S0022-1694(02)00254-8.
- Twine, T.E., Kucharik, C.J., Foley, J.A., 2004. Effects of land cover change on the energy and water balance of the Mississippi River Basin. J. Hydrometeorol. 5 (4), 640–655. https://doi.org/10.1175/1525-7541(2004)005<0640:EOLCCO>2.0.CO;2.
- U.S. Census Bureau. 2020. Census regions and divisions of the United States. Available at https://www2.census.gov/geo/pdfs/maps-data/maps/reference/us\_regdiv.pdf. Accessed 2022 May 25.
- White, R.G., Kirkegaard, J.A., 2010. The distribution and abundance of wheat roots in a dense, structured subsoil – implications for water uptake. Plant Cell Environ. 33 (2), 133–148. https://doi.org/10.1111/j.1365-3040.2009.02059.x.
- White, A.F., Schulz, M.S., Vivit, D.V., Bullen, T.D., Fitzpatrick, J., 2012. The impact of biotic/abiotic interfaces in mineral nutrient cycling: A study of soils of the Santa Cruz chronosequence, California. Geochim. Cosmochim. Acta 77, 62–85. https://doi. org/10.1016/j.gca.2011.10.029.
- Xiao, D., Brantley, S.L., Li, L., 2021. Vertical connectivity regulates water transit time and chemical weathering at the hillslope scale. Water Resour. Res. 57 (8) https:// doi.org/10.1029/2020WR029207.
- Yudina, A., Kuzyakov, Y., 2019. Saving the face of soil aggregates. Glob. Change Biol. 25 (11), 3574–3577. https://doi.org/10.1111/gcb.14779.